ΠΑΝΕΠΙΣΤΗΜΙΟ
ΘΕΣΣΑΛΙΑΣ

BSc THESIS

Study of nuclear fission fragments with artificial intelligence methods

Author:
Vasilis TSIOULOS

Supervisor:
Dr. Vaia PRASSA

A thesis submitted in fulfillment of the requirements for the degree of BSc in Physics

in the

University of Thessaly Physics Department
Lamia 2024

Εγκρίθηκε από τα Μέλη της Τριμελούς Εξεταστικής Επιτροπής:

- Πρώτο μέλος (Επιβλέπουσα)

  Βάια Πρασσά
  Επίκουρη Καθηγήτρια, Τμήμα Φυσικής, Πανεπιστήμιο Θεσσαλίας

- Δεύτερο μέλος

  Φίλιππος Σοφός
  Επίκουρος Καθηγητής, Τμήμα Φυσικής, Πανεπιστήμιο Θεσσαλίας

- Τρίτο μέλος

  Άγγελος Αβραμόπουλος
  Αναπληρωτής Καθηγητής, Τμήμα Φυσικής, Πανεπιστήμιο Θεσσαλίας

Acknowledgements

Πρώτα απ' όλα, θέλω να ευχαριστήσω την επιβλέπουσα της διπλωματικής μου εργασίας, Επίκουρη καθηγήτρια κ. Πρασσά, για την εμπιστοσύνη, την πολύτιμη βοήθεια και την καθοδήγησή της καθ'όλη την διάρκεια της εργασίας. Επίσης, ευχαριστώ και τα υπόλοιπα μέλη της εξεταστικής επιτροπής της διπλωματικής εργασίας μου, Αναπληρωτή καθηγητή κ. Αβραμόπουλο και Επίκουρο καθηγητή κ. Σοφό για την προσεκτική ανάγνωση της εργασίας μου και για τις πολύτιμες υποδείξεις τους. Οφείλω ευχαριστίες στον κ. Σοφό που με εισήγαγε στον τομέα της μηχανικής μάθησης. Επίσης, ευχαριστώ την αδερφή μου Νεφέλη για την κατανόησή της, ιδιαίτερα κατά τη διάρκεια των τελευταίων μηνών της προσπάθειάς μου. Πάνω απ' όλα, είμαι ευγνώμων στους γονείς μου, Χρήστο και Κατερίνα για την ολόψυχη αγάπη και υποστήριξή τους όλα αυτά τα χρόνια. Αφιερώνω αυτή την εργασία στην μητέρα μου και στον πατέρα μου.

Βασίλειος Τσιούλος

Περίληψη

Στην πυρηνική φυσική, η περιγραφή των Fission Product Yields (FPY) είναι κρίσιμη αλλά δύσκολη λόγω της πολύπλοκης κβαντομηχανικής φύσης των πυρηνικών αντιδράσεων. Αυτή η πτυχιακή εισάγει μηχανική μάθηση στην πυρηνική φυσική για να αντιμετωπίσει αυτές τις προκλήσεις, επικεντρώνοντας ιδιαίτερα στα FPY της πυρηνικής σχάσης. Τα θεωρητικά μοντέλα, αν και αποτελεσματικά υπό ορισμένες συνθήκες, αντιμετωπίζουν περιορισμούς στην πρόβλεψη και στη διαχείριση των τρόπων διάσπασης λόγω της περιορισμένης υπολογιστικής δύναμης. Εισάγοντας το Gaussian Process Regression (GPR) για να ξεπεράσει τους περιορισμούς, ιδιαίτερα χρήσιμη σε σενάρια με περιορισμένη διαθεσιμότητα δεδομένων. Τα πλεονεκτήματα του GPR στην αναγνώριση μοτίβων και στον υπολογισμό αβεβαιοτήτων αξιοποιούνται για να ενισχύσουν την ακρίβεια και την αξιοπιστία των προβλέψεων των FPY. Τα αποτελέσματα συμβάλλουν σημαντικά στην ανάλυση της πυρηνικής σχάσης, παρουσιάζοντας το δυναμικό της μηχανικής μάθησης για την εκλεπτυσμένη και συμπληρωματική μελέτη των μεθοδολογιών πυρηνικής φυσικής. Η εφαρμογή του GPR αποδεικνύει την πρακτική της χρησιμότητα σε περιοχές με περιορισμένα δεδομένα, προσφέροντας μια νέα προσέγγιση για μελλοντικές υπολογιστικές προόδους στην πυρηνική φυσική. Αυτή η έρευνα παρέχει όχι μόνο νέες διορατικότητες στις πολύπλοκες πυρηνικές αντιδράσεις αλλά και θέτει τις βάσεις για την ένταξη προηγμένων υπολογιστικών τεχνικών στην έρευνα της παραδοσιακής πυρηνικής φυσικής, επιτρέποντας νέες μεθόδους για την έρευνα και την εφαρμογή στον τομέα.

Abstract

University of Thessaly Physics Department

BSc in Physics

Study of nuclear fission fragments with artificial intelligence methods

by Vasilis TSIOULOS

Supervisor: Dr. Vaia Prassa, Assistant Professor

In nuclear physics, accurately modeling fission product yields (FPY) is crucial yet challenging due to the complex quantum-mechanical nature of nuclear reactions. This thesis intersects nuclear physics with machine learning (ML) to address these challenges, particularly focusing on FPY in nuclear fission processes. Traditional models, although effective in certain conditions, face limitations in predictive power and handling evolving fission modes. This research introduces Gaussian Process Regression (GPR) to overcome these limitations, especially useful in scenarios of limited data availability. GPR's strength in property prediction and uncertainty quantification is leveraged to enhance the accuracy and reliability of FPY predictions. The findings contribute significantly to the understanding of nuclear fission, showcasing the potential of machine learning to refine and complement traditional nuclear physics methodologies. The application of GPR demonstrates its practical utility in areas with constrained data, offering a novel approach for future computational advancements in nuclear physics. This research not only provides fresh insights into complex nuclear reactions but also sets the stage for integrating advanced computational techniques with traditional nuclear physics research, paving the way for enhanced scientific discovery and practical applications. The integration of machine learning, particularly GPR, in nuclear physics highlights the symbiotic relationship between computational innovation and theoretical understanding, opening new avenues for research and application in the field.

keywords: *FPY, GPR, GMM, Nuclear Fission, Fission Fragment Prediction, Data Enhancement.*

Contents

List of Figures

List of Abbreviations

FPY	**F**ission **P**roduct **Y**ields
ML	**M**achine **L**earning
AI	**A**rtificial **I**ntelligence
GPR	**G**aussian **P**roccess **R**egression
BNN	**B**ayesian **N**eural **N**etwork
MDN	**M**ixture **D**ensity **N**etwork
GMM	**G**aussian **M**ixture **M**odel
AIC	**A**kaike **I**nformation **C**riterion
BIC	**B**ayesian **I**nformation **C**riterion
BVN	**Bi**v**ariate** **N**ormal
MVN	**M**ulti**v**ariate **N**ormal
RBF	**R**adial **B**asis **F**unction
KDE	**K**ernel **D**ensity **E**stimation
JENDL	**J**apanese **E**valuated **N**uclear **D**ata **L**ibrary
MLE	**M**aximum **L**ikelihood **E**stimation
EM	**E**xpectation **M**aximization

Chapter 1

Introduction

1.1 Background Information

Nuclear fission, the process in which an atomic nucleus divides into lighter elements, releasing substantial energy, has remained an important and challenging field since its discovery over 80 years ago [1, 2]. This complex phenomenon in low-energy nuclear physics is a highly intricate, non-equilibrium quantum many-body dynamic problem. Its complexity stems from the critical influence of various nuclear matter properties and nuclear dynamics, and how they interact at different stages of the fission process. Exploring nuclear fission's mechanisms is crucial for advancing multiple areas of nuclear physics, including nuclear structure, reactions, and technology [3, 4, 5]. In heavier elements such as actinides or transactinides, fission can happen either spontaneously or be triggered by particles like neutrons. The role of spontaneous fission is significant in the stability of superheavy elements [6, 7], understanding reactor neutrinos [8], and it has a considerable impact on r-process nucleosynthesis [9, 10].

Even without the need of the fission properties for the astrophysics, nuclear fission provides a rich and diverse field for scientific exploration, encompassing a wide array of research areas in nuclear characteristics and fundamental physics. The distinct feature of fissile nuclei, which exhibit a relatively even potential energy at considerable deformations, offers a contrast to lighter nuclei. This aspect is pivotal for probing into nuclear aspects like the behavior of shell effects in states of extreme deformation. Additionally, the process of decaying quasi-bound nuclear systems past the fission barrier reveals vital insights into aspects of nuclear transport, such as the viscosity of nuclei and the dynamics of heat exchange between forming fission fragments. These studies are instrumental not only in advancing our understanding of nuclear reactions but also provide a crucial testing ground for theories on non-equilibrium processes within isolated mesoscopic systems, where the principles of quantum and statistical mechanics play a key role. This makes the study of nuclear fission a significant area of research, with implications that extend well beyond the specific domain of nuclear physics, touching upon fundamental principles of physical science.

1.1.1 Experimental information

In recent years, the field of nuclear fission has experienced a substantial increase in both experimental and theoretical activities, primarily driven by the urgent need for accurate and comprehensive nuclear data, crucial for practical applications in reactor technology. This trend highlights the significance of experimental research and the evaluation of data in enhancing reactor design and safety. A key challenge in neutron-induced fission research is the limited availability of data, especially at

various neutron energy levels, which necessitates innovative approaches to manage uncertainties. Predominant nuclear data libraries such as ENDF [11], JENDL [12], JEFF [13], and CENDL [14] primarily offer fission yield evaluations at thermal neutron energies around 0.5 MeV, but their coverage is less extensive for fast and 14 MeV high-energy neutrons. This creates a noticeable gap in data, particularly at other energy levels, limiting access to critical observables like the proton-neutron composition, total kinetic energy of fission fragments, and neutron multiplicity. Despite these challenges, recent advancements and ongoing experiments are striving to fill these gaps, focusing on aspects such as prompt-neutron spectra, fission-fragment yield cross-sections, and data on prompt-neutron and gamma emissions, which are essential for the design and operation of modern reactors [4].

1.1.2 Theoretical analysis

The theoretical modeling of fission observables remains one of the most formidable challenges in nuclear physics, as reflected in the literature [4]. Recent advancements in fully microscopic nuclear fission models, such as the time-dependent Hartree-Fock-Bogoliubov [15] and the time-dependent generator-coordinate method [16, 17, 18], can be pretty useful. However, these models are still evolving and not yet fully used for accurate quantitative applications. Alongside these, phenomenological and semimicroscopic fission models have demonstrated competence in describing existing data in certain regions. Nonetheless, their predictive power diminishes as fission modes evolve,emphasizing a significant limitation in current methodologies [19]. The complexity of fission observables arises predominantly from the intricate multidimensional potential energy surfaces, necessitating sophisticated modeling approaches.

Additionally, the fission process in compound nuclei presents the fading of quantum effects with increased excitation energies [3, 20], further complicating the theoretical landscape. Addressing the energy dependence of fission product yields (FPY) [20, 15] and post-neutron FPY (independent FPY) [21] adds another layer of complexity. Consequently, there is an increasing focus on the uncertainty quantification of nuclear models, highlighting a critical aspect of contemporary nuclear physics research [22]. Despite the strides made with these advanced models, they face challenges in precisely replicating observed data. Currently, expanding these models is a formidable task, often constrained by the need for substantial computing resources or the development of more efficient algorithms. This scenario underscores the ongoing challenges and the need for continued innovation in the field of nuclear fission modeling.

1.1.3 Machine Learning in Nuclear Physics

Statistics, data science, and ML build important fields of research in modern science. They play an important role in learning how to make predictions from data, and extract key information about physical processes and the underlying scientific laws based on large datasets. Machine learning, a subset of artificial intelligence, is now an extremely useful tool in nuclear physics, mainly due to its exceptional capability in handling large datasets and complex patterns [23]. In a field overwhelmed with large amount of data, ML algorithm's accuracy at identifying underlying relationships is pretty high and subtle differences that traditional analytical methods might miss. For instance, in experiments where the data output is massive and potentially

overwhelming, machine learning can efficiently filter through and analyze this information, extracting meaningful insights. This capability is particularly beneficial in areas like detector design, where ML can optimize sensitivity and specificity, and in the analysis where distinguishing signal from noise is crucial. This predictive power is not just limited to experimental data but also extends to theoretical models, where ML can anticipate the behavior of complex nuclear systems under various scenarios, significantly contributing to the field's advancement.

ML's also enhances computational methods in nuclear physics. Complex nuclear simulations, which are important for understanding phenomena like nuclear fission, can be incredibly computationally costly. ML algorithms can help optimize these simulations, making them more efficient and less demanding on computational resources. By learning from previous simulation outputs, ML models can predict results under new conditions with a reduced need for time consuming computation. This efficiency is crucial in broadening the nuclear research, especially in areas where computational limitations are a bottleneck [24]. In nuclear physics, accurately knowing the uncertainty in both experimental and theoretical models is necessary for the reliability of the results. ML algorithms can analyze patterns in data to identify sources of uncertainty and quantify their impact, thereby enhancing the credibility and precision of nuclear physics research.

There are two main categories of ML models, the supervised and unsupervised learning. Supervised learning, involves training a model on a labeled dataset, where the desired output, known as label for each input is known. This approach is similar to learning with a guidance, where the algorithm iteratively adjusts its parameters to minimize the difference between its predictions and the actual labels. The main benefit of supervised learning is its ability to produce highly accurate models, given sufficient and well-labeled training data. On the other hand, unsupervised learning deals with unlabeled data, aiming to uncover hidden patterns or structures within. It's like exploration without a specific target, where the algorithm tries to learn the data's properties on its own [25]. While it succeeds in discovering underlying structures and anomalies in data, unsupervised learning typically requires more data to achieve meaningful insights and often involves more complex algorithms compared to supervised learning.

Another categorization of ML is the tasks that can be used to manipulate the dataset and acquire a specific result. The two categories that are being used are the classification and regression. Classification, is a fundamental task in supervised learning that involves categorizing data into predefined classes or groups based on its features. This method is particularly effective in applications where the objective is to assign discrete labels to data instances. The success of classification models, like decision trees, support vector machines, or neural networks, is based on their ability to accurately generalize from the training data to unseen instances. On the contrary, regression focuses on predicting a continuous outcome variable based on one or more predictor variables. It is widely used for predicting numerical values. Regression models, ranging from simple linear regression to more complex methods like random forests or gradient boosting, seek to establish a relationship between the independent variables and the dependent variables, often represented by a line or curve in multidimensional space [26]. Both classification and regression are powerful tools in the ML toolkit, each suited to different types of problems depending on whether the output variable is categorical or continuous.

1.2 Goals

In the domain of machine learning applied to nuclear fission, the primary objective is to predict fission yields without relying exclusively on experimental data. Instead, a network is constructed using patterns from Nuclear Data Libraries, necessitating a probabilistic approach for uncertainty calculation and handling numerous parameters. Noteworthy networks for such applications include Bayesian Neural Networks (BNN) [27] and Mixture Density Networks (MDN) [24].

However, the challenge lies in the demand for a substantial data amount by these networks to capture correlations and provide accurate predictions. Given the limited dataset, an alternative approach is considered—constructing models that generate samples from the datasets. This strategy, avoiding the complexity of deep learning models, aims to evaluate and compare models based on their ability to capture yield distributions [28]. Addressing this challenge, the main objective of this thesis emerges: to initiate research into predicting FPY using a targeted approach in data analysis, particularly leveraging the Japanese Evaluated Nuclear Data Library (JENDL).

This attempt begins with the generation of sample datasets from JENDL by employing two widely recognized Gaussian networks: the Gaussian Mixture Model (GMM) and the GPR. The use of GMM for sampling in the context of FPY prediction was previously explored by Lovell et al. [29], who utilized Mixture Density Networks (MDN) to discern Gaussian function parameters pertinent to FPY prediction. Building upon the accuracy insights from GMM sampling demonstrated by Lovell et al., this research attempts to sample both charge and mass yield datasets from JENDL [30]. For charge yields, the focus is on sampling specific nuclei, including ^{244}Cm at 0.5 MeV, ^{255}Fm at thermal neutron energies, ^{256}Fm, ^{239}Pu at 14 MeV, ^{233}U at 14 MeV, and ^{235}U at 14 MeV. The mass yields being sampled encompass nuclei such as ^{252}Cf, ^{246}Cm, ^{246}Cm at 0.5 MeV, ^{232}Th at 0.5 MeV, ^{235}U at 0.5 MeV, and ^{238}U.

The chosen dataset includes mass and charge yields of induced and spontaneous fission events. In the case of induced fission we selected thermal energies of neutrons, neutron energies 0.5 MeV and 14 MeV from JENDL. This approach not only seeks to validate and extend the findings of previous research but also aspires to offer new insights into the predictive capabilities of machine learning models in the domain of nuclear data analysis.

Training the GMM and extracting samplings is generally considered more straightforward compared to the GPR. This relative ease with the GMM primarily stems from its simpler hyperparameter tuning process, where the primary variable is the number of Gaussian components used in the model. The components is the main hyperparameter that takes place in the classification task, as they define the complexity and flexibility of the model in capturing the underlying patterns in the dataset. By adjusting the number of Gaussians, the GMM can be fine tuned fast and with accuracy, making it an effective tool for classification tasks in nuclear data analysis.

On the other hand, GPR, even though they both work with gaussian distributions, they differ a lot in structure but mainly in complexity. Its capability to calculate uncertainties within the dataset makes it particularly suitable for more nuanced analytical tasks, such as predicting single fission yields. GPR has has the ability to model the underlying function that appears in the dataset, providing useful predictions and confidence intervals. This feature is extremely valuable in nuclear physics, where understanding the uncertainty and reliability of experimental data is as crucial as the data itself. Taking advantage of GPR to single fission yields, it allows for a more sophisticated evaluation of experimental data, enabling the creation of

highly accurate and reliable samplings. The intricacy of GPR's hyperparameter tuning, which includes parameters like length scales and variance, requires a deeper understanding of the data and the model, but it offers a more detailed and insightful analysis, particularly valuable in the field of nuclear data analysis.

In the present thesis, two models from the Scikit-learn Python library, the GMM and GPR, are employed to analyze nuclear data. Each model has its specific strengths and applications in the context of extracting samples from the dataset. The GPR is excellent at solving regression problems and in predicting uncertainties, a feature that is crucial in the field of nuclear data. This capability of GPR makes it pretty useful tool in the analysis of fission yields, allowing for a more demanding and reliable understanding of the data.

The GMM, even if we take into consideration it's effectiveness of segmenting the dataset into distinct Gaussian distributions, it lacks the inherent ability to predict uncertainties associated with these distributions. Despite this, the GMM is important in exploring and handling the correlations present within the nuclear data, providing a clear understanding of the underlying distribution patterns. This differentiation in capabilities between GMM and GPR is the motivation of this work. By testing the strengths of both models, the thesis aims to investigate the correlations throughout the entire dataset of fission yields in Nuclear Data Libraries, using GPR for its predictive accuracy in uncertainties and GMM for its ability in data clustering and pattern recognition.

Chapter 2

Models

2.1 Gaussian Mixture Model

2.1.1 Definition and surface analysis

The Gaussian Mixture Model is a clustering method based on unsupervised learning, which means that the dataset is unlabeled, and the algorithm tries to learn the patterns and relationships in the data without any explicit guidance. Unsupervised learning in general is the training of the model, using information that is neither classified nor labeled and allow the algorithm to act on that information without guidance in Chapter 1.

Clustering is a data analysis technique that involves grouping similar data points together to uncover patterns within a dataset. Various clustering methods exist, each with its own approach to partitioning the data into distinct clusters based on similarities or distances between data points. These methods include K-means, hierarchical clustering, and density-based clustering algorithms. The choice of clustering method depends on factors such as data distribution, interpretability of clusters, and computational efficiency. For the type of distribution of our dataset, the GMM is superior to the K-means. Due to the non-linear distribution and the scarceness of datapoints in our dataset, this probabilistic model is a better fitted approach than the K-means. The GMM is thoroughly described in Ref. [31, 32, 33]. Its main goal is to cluster data points by applying gaussian distributions, returning the gaussian parameters, mean μ and standard deviation σ.

To illustrate GMM, we start with a simple example of a clustering problem. In figure 2.1 the dataset can be clearly distinguished into two clusters.

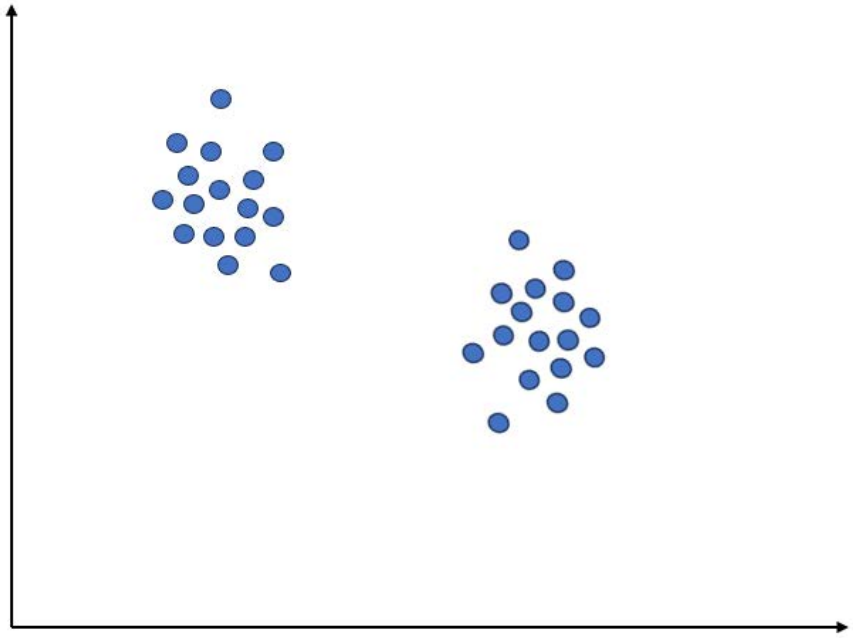

FIGURE 2.1: An example of clustered dataset

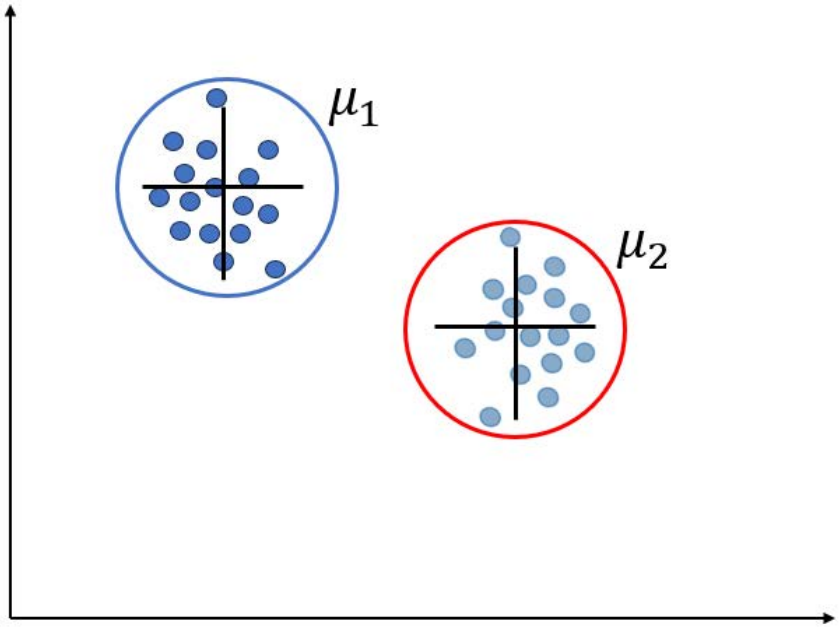

FIGURE 2.2: Dividing Clusters

The parameters μ_1 and μ_2, in Fig. 2.2 represent the central locations of clusters. In GMM, the function is composed of multiple Gaussian distributions, each denoted by K, which corresponds to the number of clusters. Within each Gaussian, there are three key elements: a mean that locates the center, a covariance matrix determining the cluster's spread, and a mixing probability that specifies the relative size of the Gaussian distribution. For a dataset comprising two clusters, each cluster is modeled as a separate Gaussian function [34].

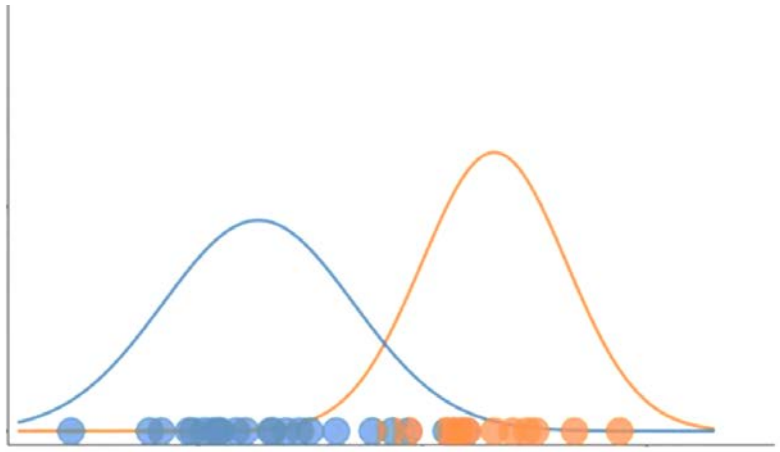

FIGURE 2.3: 2 Gaussian functions

The mixing probability is defined by the equation:

$$\sum_{k=1}^{K} \pi_k = 1 \tag{2.1}$$

The multivariate normal distribution, commonly referred to as the Gaussian Density Function, is characterized by a specific mathematical expression:

$$\mathcal{N}(x|\mu,\Sigma) = \frac{1}{(2\pi)^{D/2}|\Sigma|^{1/2}} exp(-\frac{1}{2}(x-\mu)^T\Sigma^{-1}(x-\mu)) \tag{2.2}$$

In the general form of the multivariate normal distribution, the variable x signifies the data points being considered. $\boldsymbol{D}$ represents the dimensionality of each data point. The terms μ and Σ correspond to the mean vector and the covariance matrix, respectively, of the distribution. For a dataset comprising $N = 1000$ two-dimensional points ($D = 2$), where each data point is denoted by the vector $\mathbf{x}$, the dimensions of the relevant parameters are as follows:

- $\mathbf{x}$: A matrix with dimensions 1000×2, where each row corresponds to a data point and each column corresponds to a dimension.
- $\boldsymbol{\mu}$: A vector with dimensions 1×2, representing the mean of the data points across the two dimensions.
- $\boldsymbol{\Sigma}$: A matrix with dimensions 2×2, representing the covariance matrix of the data points.

For analytical purposes, it can be beneficial to consider the logarithmic form of the multivariate normal distribution. The logarithm of this distribution is expressed as follows:

$$\log P(\mathbf{x}) = -\frac{D}{2}\log(2\pi) - \frac{1}{2}\log|\boldsymbol{\Sigma}| - \frac{1}{2}(\mathbf{x}-\boldsymbol{\mu})^T\boldsymbol{\Sigma}^{-1}(\mathbf{x}-\boldsymbol{\mu}) \tag{2.3}$$

By taking the derivatives of the logarithmic form of the multivariate normal distribution with respect to both the mean and covariance, and setting these derivatives to zero, we can determine the optimal values for these parameters. These solutions

represent the Maximum Likelihood Estimates (MLE) for the mean and covariance in this scenario. However, the complexity increases when dealing with multiple Gaussian distributions as opposed to just one. In order to find the parameters for the entire mixture, additional considerations are required. These will be explored in the following section.

2.1.2 Mathematical analysis

Let $\boldsymbol{z}$ be the set of all possible latent variables z. Hence:

$$\boldsymbol{z} = \{z_1, ..., z_K\} \tag{2.4}$$

If we deduce the likelihood of our observed data being derived from the Gaussian k, we arrive at a conclusion that mirrors the Gaussian function itself.

$$p(x_n|z) = \prod_{k=1}^{K} \mathcal{N}(x_n|\mu_k, \Sigma_k)^{z_k} \tag{2.5}$$

The recently deduced equations, in conjunction with Bayes' theorem, provide a method to determine this probability. By applying the rule of product in probability theory, we arrive at the following expression:

$$p(x_n|z) = p(x_n|z)p(z) \tag{2.6}$$

The subsequent stage involves eliminating the variable z from **eq.** (2.6). This is achieved through the application of the marginalization process, which essentially entails summing over the terms related to the variable z:"

$$p(x_n) = \sum_{k=1}^{K} p(x_n|z)p(z) = \sum_{k=1}^{K} \pi_k \mathcal{N}(x_n|\mu_k, \Sigma_k) \tag{2.7}$$

The equation in question delineates a Gaussian Mixture, clearly dependent on all the parameters discussed earlier. To pinpoint the most suitable values for these parameters, it's imperative to determine the model's maximum likelihood. This likelihood is calculable as the joint probability of all observations x_n, characterized by the following definition:

$$p(X) = \sum_{n=1}^{N} p(x_n) = \prod_{n=1}^{N} \sum_{k=1}^{K} \pi_k \mathcal{N}(x_n|\mu_k, \Sigma_k) \tag{2.8}$$

If we apply the log in the equation, hence:

$$\ln p(X) = \sum_{n=1}^{N} \ln \sum_{k=1}^{K} \pi_k \mathcal{N}(x_n|\mu_k, \Sigma_k) \tag{2.9}$$

To estimate the parameters, we must resort to an iterative approach. However, before we advance, remember our initial objective was to ascertain the probability of z given x. With all the requisite components now at our disposal, we are equipped to articulate the form of this probability. Therefore, employing Bayes' theorem, we

proceed as follows:

$$p(z_k = 1|x_n) = \frac{p(x_n|z_k = 1)p(z_k = 1)}{\sum_{j=1}^{K} p(x_n|z_j = 1)p(z_j = 1)} \tag{2.10}$$

with $p(z_k = 1) = \pi_k$ and $p(x_n|z_k = 1) = N(x_n|\mu_k, \Sigma_k)$:

$$p(z_k = 1|x_n) = \frac{\pi_k N(x_n|\mu_k, \Sigma_k)}{\sum_{j=1}^{K} \pi_j \mathcal{N}(x_n|\mu_j, \Sigma_j)} \tag{2.11}$$

We have now derived formulas for probabilities that are critical in calculating the parameters of our model. As noted earlier, directly computing (2.9) to obtain these parameters is a complex task. To tackle this challenge utilize an iterative solution, the Expectation-Maximization (EM) algorithm. This algorithm is frequently used in optimization scenarios involving intricate objective functions, which is analogous to the situation we face with GMM. The parameters defining the Gaussian distribution include:

$$\theta = \{\pi, \mu, \Sigma\}$$

We can begin with our results from the K-means that ran on the dataset, see Fig. 2.2, and then initialize the θ parameters. Then we evaluate the results:

$$Q(\theta^*, \theta) = E[\ln p(X, Z|\theta^*] = \sum_{Z} p(Z|X, \theta) \ln p(X, Z|\theta^*) \tag{2.12}$$

If we assume that (2.11)=$\gamma(z_{nk})$, for evaluation, we must caclulate the $\gamma(z_{nk})$ with the old parameters, so if we replace the (2.11) to (2.12), we will have:

$$Q(\theta^*, \theta) = \sum_{Z} \gamma(z_{nk}) \ln p(X, Z|\theta^*) \tag{2.13}$$

The only missing part from the equation is the $p(X, Z|\theta^*)$. This part represents the complete likelihood of the model, encompassing both X and Z. This can be determined by utilizing the following expression:

$$p(X, Z|\theta^*) = \prod_{n=1}^{N} \prod_{k=1}^{K} \pi^{z_{nk}} N(x_n|\mu_k, \Sigma_k)^{z_{nk}} \tag{2.14}$$

The equation that occurred is the joint probability of all observations and variables, with the log expression of this equation to be:

$$\ln p(X, Z|\theta^*) = \sum_{n=1}^{N} \sum_{k=1}^{K} z_{nk}[\ln \pi_k + \ln N(x_n|\mu_k, \Sigma_k)] \tag{2.15}$$

All these efforts were made to simplify the estimation of the parameters. By maximizing the function Q with respect to θ, one can compute the parameters. It's also important to recognize that the latent variable z will consistently equal 1 during each summation evaluation. With this insight, we can conveniently disregard it as needed in our calculations. If we now merge (2.15) to (2.13), we get:

$$Q(\theta^*, \theta) = \sum_{n=1}^{N} \sum_{k=1}^{K} \gamma(z_{nk})[\ln \pi_k + \ln N(x_n|\mu_k, \Sigma_k)] \tag{2.16}$$

Nonetheless, Q must consider the constraint that the sum of all π values should equal one. To accommodate this requirement, we will introduce an appropriate Lagrange multiplier.

$$Q(\theta^*, \theta) = \sum_{n=1}^{N} \sum_{k=1}^{K} \gamma(z_{nk})[\ln \pi_k + \ln N(x_n|\mu_k, \Sigma_k)] - \lambda(\sum_{k=1}^{K} \pi_k - 1) \tag{2.17}$$

Now, we can readily ascertain the parameters using maximum likelihood. Let's proceed by taking the derivative of Q with respect to π and equating it to zero:

$$\frac{\partial Q(\theta^*, \theta)}{\partial \pi_k} = \sum_{n=1}^{N} \frac{\gamma(z_{nk})}{\pi_k} - \lambda = 0 \tag{2.18}$$

By solving for λ and applying summation for k we get:

$$\sum_{n=1}^{N} \gamma(z_{nk}) = \pi_k \lambda \Rightarrow \sum_{k=1}^{K} \sum_{n=1}^{N} \gamma(z_{nk}) = \sum_{k=1}^{K} \pi_k \lambda \tag{2.19}$$

From this point and on, to find the parameters of θ, we can solve for π from the (2.19), or differentiate Q with respect to μ or Σ.

$$\left\{ \begin{array}{l} \pi_k = \frac{\sum_{n=1}^{N} \gamma(z_{nk})}{N} \\ \mu_k^* = \frac{\sum_{n=1}^{N} \gamma(z_{nk}) x_n}{\sum_{n=1}^{N} \gamma(z_{nk})} \\ \Sigma_k^* = \frac{\sum_{n=1}^{N} \gamma(z_n k)(x_n - \mu_k)(x_n - \mu_k)^T}{\sum_{n=1}^{N} \gamma(z_{nk})} \end{array} \right\}$$

2.1.3 Model Selection

In GMM, model selection is a critical step to determine the optimal number of components (Gaussians) that best represent the data. This selection is not straightforward, as a balance between model complexity and fit is crucial. Overly complex models may overfit, while overly simple ones may underfit. Techniques like the Akaike Information Criterion (AIC) and Bayesian Information Criterion (BIC) are instrumental in this context. They provide quantifiable measures to compare different models, guiding the selection of a model that appropriately captures the underlying data structure without unnecessary complexity. Model selection in GMM plays a critical role in data analysis as discussed in Refs. [35, 36].

AIC evaluates a model based on the information loss. It combines the model's accuracy with a penalty for increased complexity (number of parameters). A lower AIC value suggests a better model. AIC is given by the formula:

$$AIC = 2k - 2 \ln \hat{L} \tag{2.20}$$

where k is the number of parameters in the model and $\hat{L}$ is the maximized value of the likelihood function for the model. The term $2k$ penalizes complexity, while $-2 \ln \hat{L}$ represents model fit.

BIC is similar to AIC but applies a larger penalty for complexity, especially in models with larger datasets. Like AIC, a lower BIC value indicates a preferable

model.The Bayesian Information Criterion is computed as:

$$BIC = \ln(n)k - 2\ln\hat{L} \tag{2.21}$$

Here, n is the number of data points, k is the number of parameters, and $\hat{L}$ is the maximized likelihood. The term $\ln(n)k$ introduces a harsher penalty for models with more parameters, especially as the dataset size increases.

The optimal number of components used in the gaussian mixture can be easily achieved by using a brute-force technique, which is using a random number of gaussians to check whether the $\hat{L}$ is maximized. In Fig. 2.4, the optimal number of gaussians is identified by the elbow that appears at the minimum point of the Information Criterion (number of components equals 9).

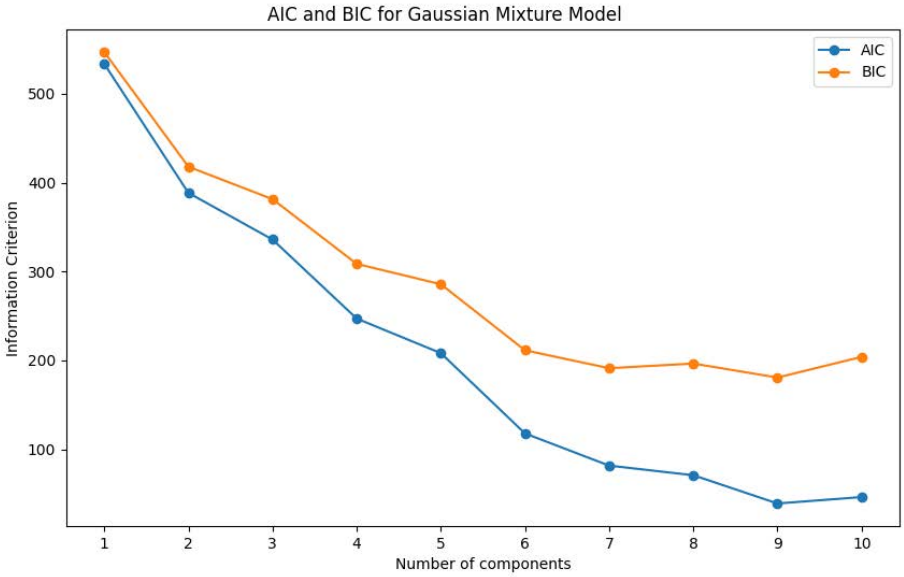

FIGURE 2.4: AIC and BIC example on number of components for ^{252}Cf.

2.2 Gaussian Process Regression

2.2.1 Definition

Gaussian Process Regression, [37, 38, 39] is a sophisticated probabilistic algorithm within the ML landscape, categorized under supervised learning. This approach is non-parametric and leverages kernel-based methods, aimed at regression tasks to predict continuous outcomes.

Unlike unsupervised learning, as used in GMM, GPR employs supervised learning. Through supervised learning, GPR models are trained to recognize and associate various patterns in the input data with their respective outputs, thereby gaining a refined understanding of the relationships within the data.

2.2.2 Kernel Methods

A key feature of GPR is its use of kernel methods, a crucial component in its model architecture. Kernel methods are a group of algorithms that are being used for pattern analysis, with the ability of mapping input data into a higher-dimensional feature space. This maps the model to perform linear regression in a more complex space [30].

The kernel is a function that calculates the similarity between pairs of data points in the input space, transforming the data into a higher-dimensional space without the need for external computation of these new coordinates. This technique allows the model to handle easily non-linear relationships, improving its capacity to deal with various complex regression tasks.

In conclusion, GPR combines supervised learning with the functionality of kernel methods. Its potential is providing uncertainty measures for predictions, crucial in decision-making processes where the confidence level of predictions is as important as the predictions themselves [30].

2.2.3 Mathematical analysis

The objective of GPR is to perform regression on a set of data points by establishing a distribution across a potentially infinite array of functions. This approach allows GPR to fit the given data points effectively. To start with, we adopt a Gaussian distribution with a mean μ and a variance σ^2, with the equation of the gaussian to be:

$$P(x) = \frac{1}{\sqrt{2\pi}\sigma} \exp\left(-\frac{(x-\mu)^2}{2\sigma^2}\right) \tag{2.22}$$

With this equation, we can give it random data points in order to capture the gaussian distribution in a Probability Density Function.

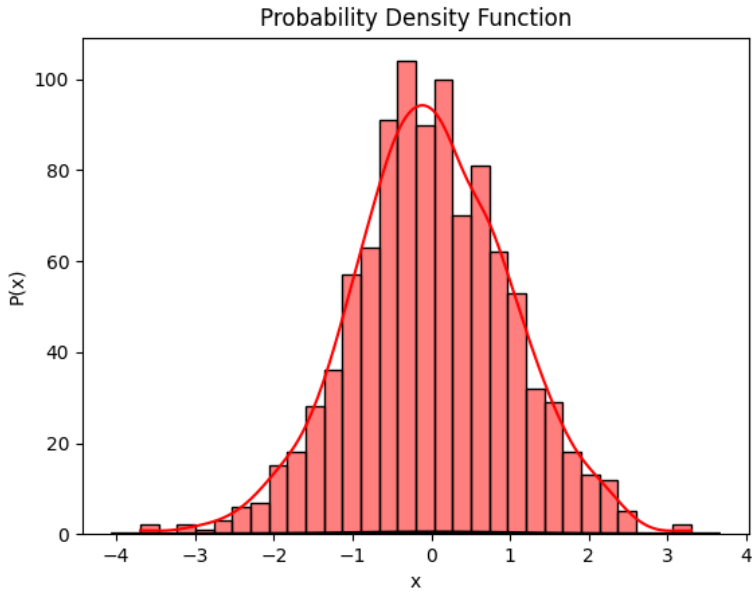

FIGURE 2.5: Data points fitted into Probability Density Function

We can label the data points from Figure 2.5 as $x_1 = [x_1^1, x_2^2, ..., x_1^n]$ for future reference. The variables input network variables the network are often interrelated. To capture these correlations and model them using a Gaussian model, we employ a multivariate Gaussian/Normal distribution model, which is defined as:

$$\mathcal{N}(x|\mu,\Sigma) = \frac{1}{(2\pi)^{D/2}|\Sigma|^{1/2}} \exp\left[-\frac{1}{2}(x-\mu)^T\Sigma^{-1}(x-\mu)\right] \tag{2.23}$$

Here D represents the number of dimensions, μ denotes the mean, and Σ stands for the covariance matrix. The covariance matrix is a symmetric matrix that stores the pairwise covariance between all the random variables being jointly modeled.

We use a bivariate normal (BVN) distribution as a simplified example to understand the theory of multivariate normal (MVN) distributions. A BVN distribution can be visualized as a three-dimensional (3D) bell curve, where the heights represent the probability density. The projections of this 3D bell curve onto the x_1 and x_2 plane are displayed as elliptical contours. The shapes of these ellipses depict the correlations between x_1 and x_2 points, illustrating how one variable in x_1 is related to another variable in x_2.

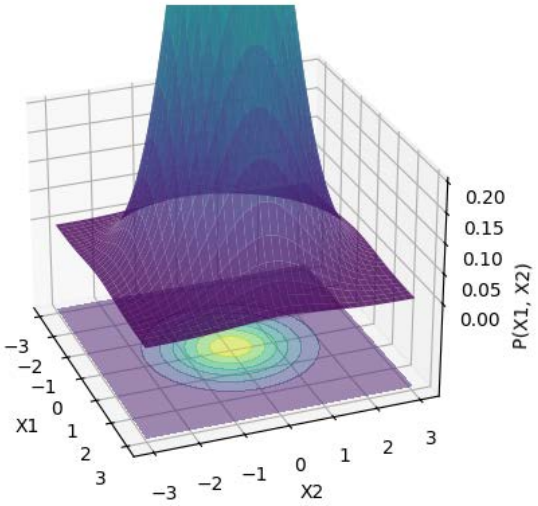

FIGURE 2.6: PDF and bi-variate normal distribution (BVN).

The $P(x_1, x_2)$ is the joint probability of x_1 and x_2. For a BVN, the mean vector $\boldsymbol{\mu}$ is a two-dimensional vector represented as $\begin{bmatrix}\mu_1\\ \mu_2\end{bmatrix}$, where μ_1 and μ_2 are the separate means for x_1 and x_2, respectively. The covariance matrix is denoted as $\begin{bmatrix}\sigma_{11} & \sigma_{12}\\ \sigma_{21} & \sigma_{22}\end{bmatrix}$, with the diagonal elements σ_{11} and σ_{22} representing the individual variances for x_1 and x_2, respectively. The off-diagonal terms σ_{12} and σ_{21} represent correlations between x_1 and x_2 and equals to the distribution $\mathcal{N}(\mu, \Sigma)$.

It is understandable that we need conditional probability rather than the joint probability for regression tasks. If we cut a slice on the 3D bell curve, we get the conditional probability distribution $P(x_1|x_2)$. Notably, the conditional distribution also follows a Gaussian distribution.

2.2.4 Kernel Analysis

At the heart of GPR are kernel functions, which define the covariance between pairs of random variables in the Gaussian process. The choice of kernel significantly impacts the model's performance and its ability to generalize from training data to unseen data. Kernels encode assumptions about the function that the model is trying to learn, and different kernels can capture different types of patterns and relationships in the data. The selection of kernels in this analysis is quite deliberate, as each of the kernels employed plays a pivotal role in predicting the bimodal distribution of fission yields. Our exploration of these kernels begins with the simplest one, known as the constant kernel. As its name implies, this kernel assumes a constant covariance across the input space. While it may not seem useful on its own, it can be valuable when combined with other kernels to model functions with varying means. The equation of the kernel is as simple as its name:

$$k(x, x^{'}) = \sigma^2 \tag{2.24}$$

Where $sigma^2$ is the constant variance.

Moving on to the next kernel, one of the most important ones in this analysis, is the radial basis function (RBF) kernel, also known for its bell-shaped curve, often referred to as the squared exponential kernel. Its use can be characteristic to its smoothness and infinite differentiability. The assumption of this kernel is that points in proximity within the input space appear higher levels of correlation. This property makes it an excellent choice for modeling functions characterized by smoothness and continuity.

Analyzing further, the RBF kernel is very good in capturing gradual transitions and variations in data, making it appropriate for tasks where the relationships are expected to be smooth and continuous. Its ability to represent complex patterns in the dataset is the reason behind its popularity in ML applications. In summary, the RBF kernel's combination of smoothness, infinite differentiability, and the assumption of higher correlation among nearby points make it a valuable tool for modeling various phenomena, especially when dealing with data exhibiting gradual variations and continuity. Hence, it's equation is:

$$k(x, x^{'}) = \exp -\frac{||x - x^{'}||}{2l^2} \tag{2.25}$$

Here l is the length-scale parameter.

The rational quadratic kernel, as an extension of the RBF kernel, offers an alternative approach to modeling data patterns. It can be seen as a blend of RBF kernels with distinct characteristic length-scales, allowing the model to adapt to datasets that exhibit scales of variation. This adaptability enables the model to effectively capture both local fluctuations and broader global within the data. By incorporating multiple kernels with different length-scales, the kernel enhances its capacity to handle patterns of variation, making it well-suited for addressing data challenges where complexities in data dynamics are the norm. The equation of the kernel resembles a bit the RBF kernel:

$$k(x, x^{'}) = \left(1 + \frac{||x - x^{'}||^2}{2\alpha l^2}\right)^{-\alpha} \tag{2.26}$$

where α controls the scale mixture and l is the length-scale.

Last but not least, the ExpSineSquared kernel stands out due to its ability to model periodic functions, making it a valuable tool for handling data with complex patterns. Its capability becomes advantageous when dealing with datasets that display consistent and periodic behavior. By accurately capturing the data distriution, this kernel is crucial for understanding the patterns, which can be a chalenging task for alternative kernel functions.

Analyzing further, the ExpSineSquared kernel operates by incorporating a sinusoidal component, which aligns with the fundamental characteristics of periodic phenomena often observed in various domains. Its ability to adapt to and represent these periodic variations enhances its applicability in fields such as signal processing and time series analysis. In essence, this kernel offers a customized solution for tasks where the underlying data exhibits regular cyclic behavior, providing a powerful tool for capturing the correlations of periodic patterns. For the equation, as the name gives up its form is:

$$k(x, x^{'}) = \exp\left(-\frac{2\sin^2(\pi|x - x^{'}|/p)}{l^2}\right) \tag{2.27}$$

where l is the length-scale and p is the periodicity.

Analyzing these kernels both mathematically and visually through figures can provide deeper understanding into their behavior for different types of datasets. Graphical representations can be particularly illuminating, showing how each kernel responds to variations in the data. So by plotting the shapes of these kernels, we can show the dependence of each kernel.

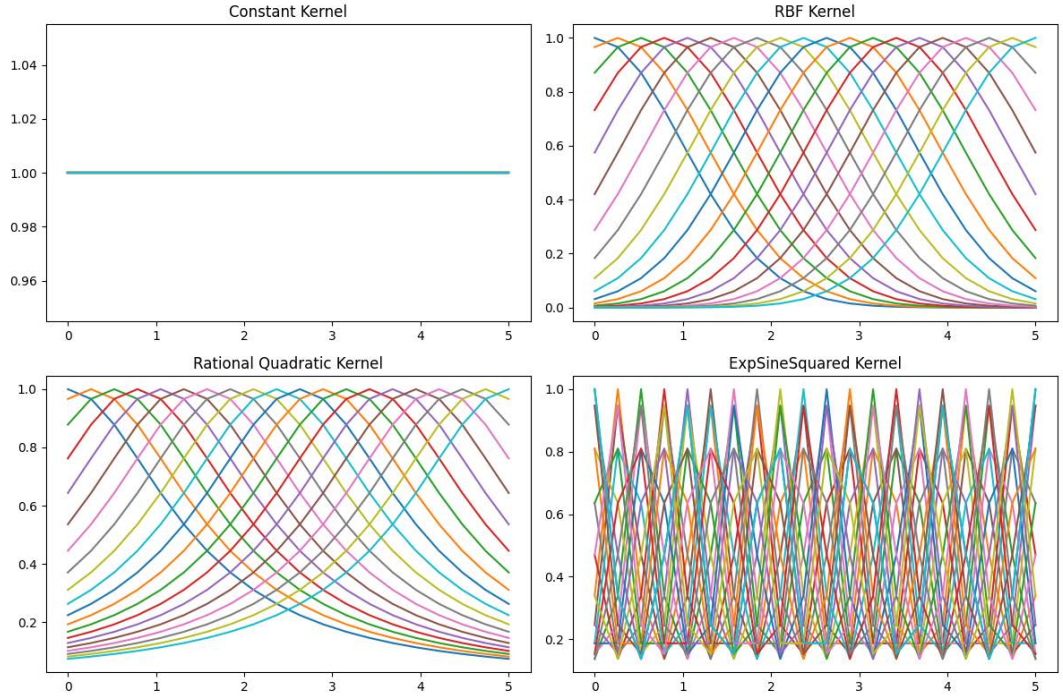

FIGURE 2.7: Different Kernel forms.

By integrating these kernels and fine-tuning their associated hyperparameters, it becomes possible to achieve highly accurate predictions, even in scenarios where datasets are limited in size, and the underlying distribution equation remains undisclosed. With this in mind, we conducted a test using the mass yields of the fissioning nucleus ^{252}Cf, and the outcome was as follows:

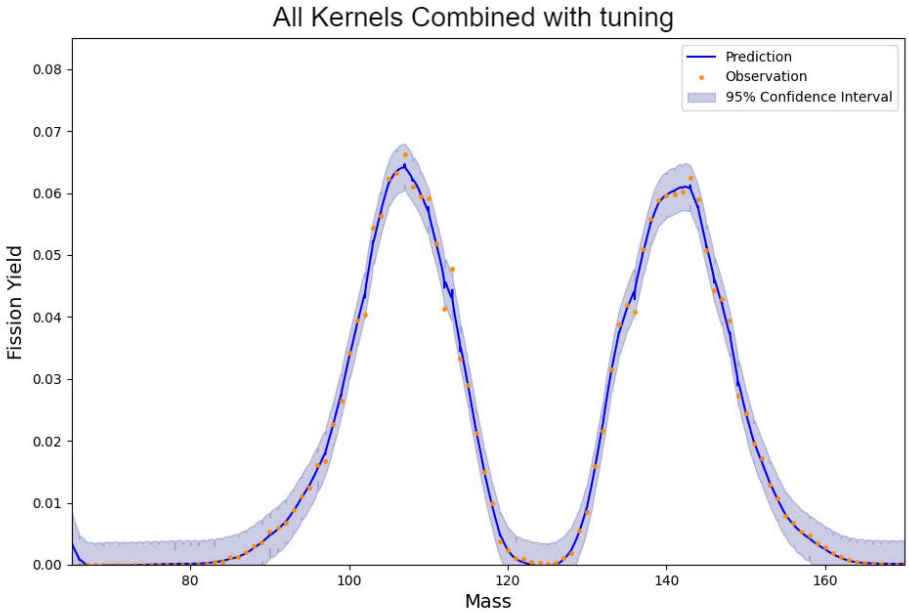

FIGURE 2.8: Combination of all kernels on the Spontaneous Fission of ^{252}Cf.

Chapter 3

Results

In this section, we detail the key findings of our study, which primarily centers on the innovative use of GMM and GPR within the field of nuclear physics, with a particular focus on predicting fission yields. Utilizing GMM, we generated 10000 samples from the experimental data, preparing them for integration into more complex probabilistic models like BNNs and MDNs. Subsequently, we employed GPR to model the multi-modal distributions of the data and to quantify their uncertainties. Following the predictions, we extracted samples from the trained network, mirroring the approach taken with GMM. The efficacy of these sampling methods, both from GMM and the trained network, was then evaluated against the experimental data to ascertain which model more accurately captured the dataset's distribution.

3.1 Gaussian Mixture Model

Beginning our analysis, we focused on the functionality of GMM. With this aim, we utilized the AIC and the BIC to ascertain the most appropriate number of Gaussian components for accurately representing the distribution. Fig. 3.1 shows the optimal number of components, number of Gaussians, for the AIC and BIC for the mass yields of each fissioning nucleus, offering a visual understanding of the model selection criteria.

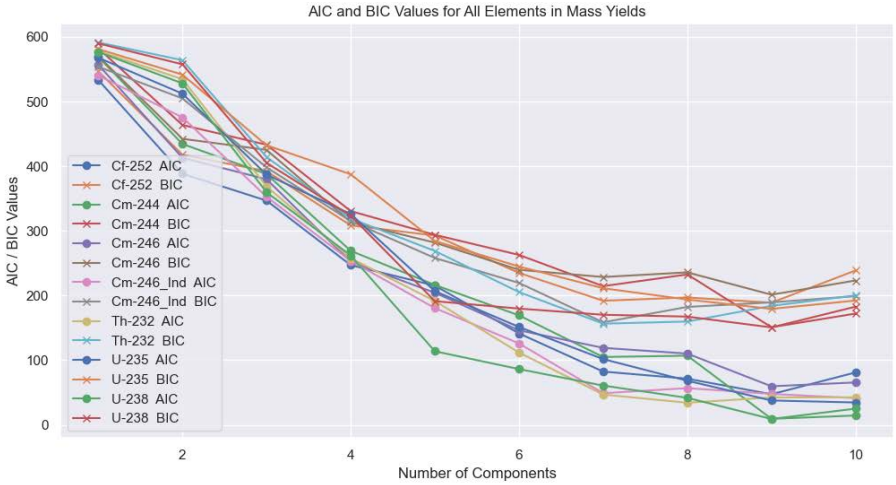

FIGURE 3.1: AIC and BIC values in respect of the number of Gaussians for each element used in mass yields dataset

The results presented in Fig. 3.1 indicate that, in most instances, the optimal number of Gaussian components for our analysis lies between 7-9, where the figure

appears to have an elbow. This observation is derived from evaluating both the AIC and BIC values across different cases. Notably, in some cases, the model demonstrated enhanced performance in capturing the distribution when guided by these AIC and BIC metrics. Here the best results were obtained for ^{244}Cm and ^{238}U.

The same process is repetead for the fission charge yields.

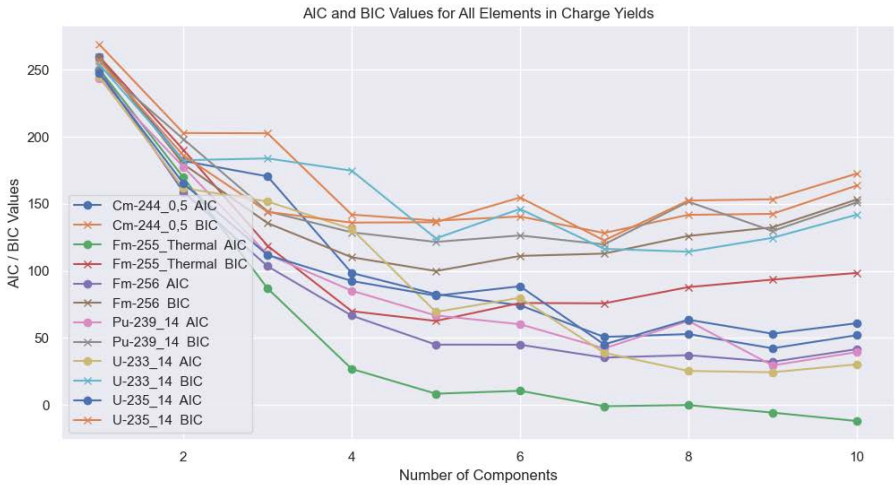

FIGURE 3.2: AIC and BIC values in respect of the number of Gaussians for each element used in charge yields dataset.

The results shown in Fig. 3.2, mirror those of mass yields and reveal intriguing insights, especially in the context of the JENDL library's data on charge yields, which contains half the number of data points than the mass yields. Despite this reduced dataset, GMM demonstrated superior effectiveness in capturing the distribution compared to the mass yields. The optimal number of Gaussian components, as discerned from Fig. 3.2, falls within the range of 8 to 10, as it can be seen by the elbow that appears at the end of the figure.

The efficacy of GMM in dealing with distributions of charge yields, such as in the case of ^{255}Fm, which follow a binomial Gaussian distribution, can be attributed to its clustering approach. This method typically produces favorable outcomes, particularly when the data displays smoothness and comprises a smaller number of data points. The relatively simple structure of the data in such cases enables GMM to accurately capture the distribution.

Overall, the utility of GMM extends beyond traditional applications and is increasingly recognized in the realm of computationally demanding Neural Networks. Its efficiency in identifying the optimal method for data sampling, while incurring a low computational cost, makes GMM a valuable tool in advanced machine learning processes. This synergy between GMM and Neural Networks underscores the evolving landscape of computational methods in data analysis and model optimization.

3.2 Gaussian Process Regression

The second method, Gaussian Process Regression, is employed not only for sampling purposes but also for predicting fission yields. GPR's adaptability, especially due to kernel optimization, allows it to address complex regression tasks effectively, which also enables subsequent sampling of the results. This adaptability is crucial in handling the complexities inherent in nuclear physics data.

However, GPR limitations, particularly its modeling approach, while effective in certain scenarios, may not be ideal for integrating a wide range of parameters, such as excitation energy and mass yields of each fragment. This limitation stems from GPR's inherent modeling strategy, which might not be as effective in capturing more intricate relationships that are crucial in this field.

Despite GPR's superiority in offering high-quality predictions of yields, there are instances where its application alone might not suffice. In such cases, a more advanced approach, like probabilistic neural networks, becomes essential. These networks are capable of learning from a diverse set of inputs, thus providing a more comprehensive model. They can uncover complex interdependencies within the input variables, offering a richer understanding and more accurate predictions.

To summarize, while GPR is a powerful tool for predicting fission yields, especially due to its flexibility in managing regression challenges, it may not always capture the entire spectrum of complex relationships in the data.

3.2.1 Mass Yields

The prediction of local corellations of mass yields is a critical aspect in the field of nuclear physics, especially when it comes to understanding fission processes and quality of the data. By using GPR, one can make accurate predictions about the distribution of yields in nuclear fission events. This is particularly important for experiments where direct measurements are challenging or impossible. GPR, with its ability to model complex, non-linear relationships in data, allows for the estimation of yields based on known properties and measurements. Additionally, GPR provides a quantification of the inherent uncertainty present in the data, thereby enhancing our understanding of potential errors.

We used the mass yields from JENDL for cases of 6 nuclei undergoing both spontaneous and induced fission at different neutron energies. For induced fission, the nuclei analyzed are Curium-246 (^{246}Cm) at a neutron energy of 0.5 MeV, Thorium-232 (^{232}Th) also at 0.5 MeV neutron energy, and Uranium-235 (^{235}U) exposed to thermal neutron energy. On the other hand, the nuclei selected for studying spontaneous fission include Californium-252 (^{252}Cf), ^{246}Cm, and Uranium-238 (^{238}U).

The cases we first studied was the spontaneous fission of ^{252}Cf and the induced fission of ^{232}Th at 0.5 MeV. The results of the GPR are seen in Figs. 3.3, 3.4.

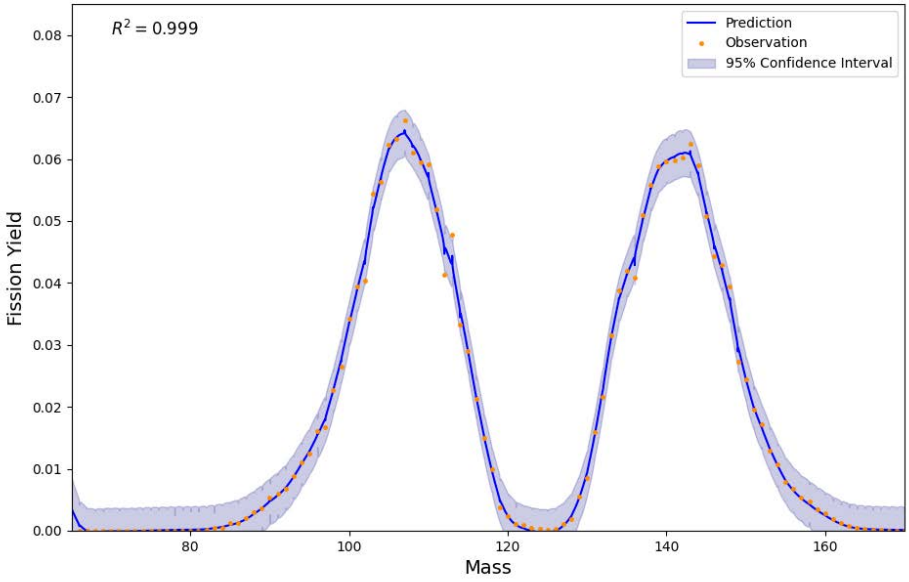

FIGURE 3.3: The mass yield prediction of GPR for Spontaneous fission of ^{252}Cf

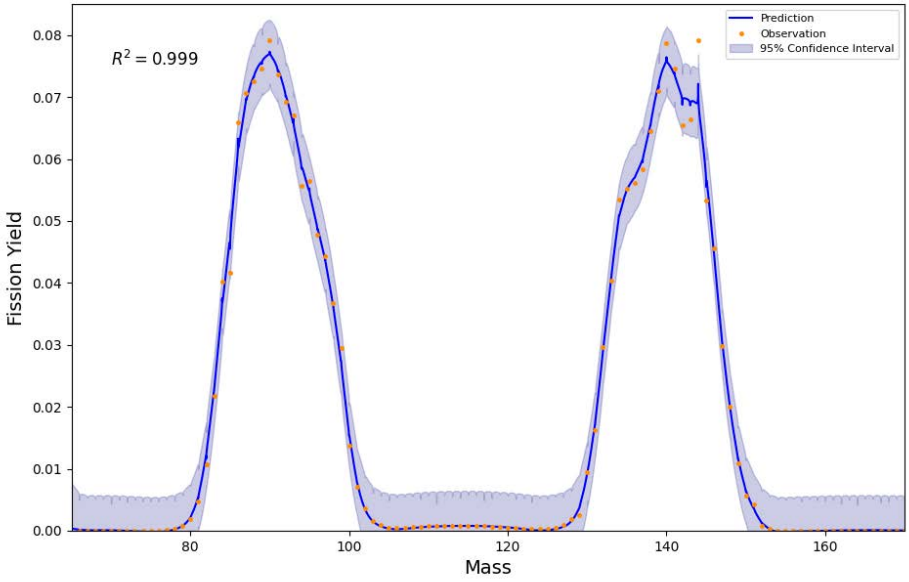

FIGURE 3.4: The mass yield prediction of GPR for Induced fission of ^{232}Th

The fig. 3.3 of nucleus ^{252}Cf exhibits a more refined and smoother prediction with a superior confidence interval compared to the induced fission cases. This distinction can be attributed to the smoother data distribution characteristic of ^{252}Cf. Unlike ^{232}Th, the data for ^{252}Cf aligns more closely with a Gaussian distribution,

allowing for easier identification and modeling without the need for highly sophisticated regression tools.

We focus on the same element with differing mass numbers, as seen in the case of Uranium. Here, we compare ^{235}U, which is subject to induced fission, with ^{238}U, known for undergoing spontaneous fission. This comparison is crucial in understanding how a change in mass number, even within the same element, can have a significant impact on the nature of fission and the resulting mass . It sheds light on the distinct nuclear reactions and fission processes that are influenced by isotopic variations, enhancing our yields comprehension of the intricate aspects of nuclear physics.

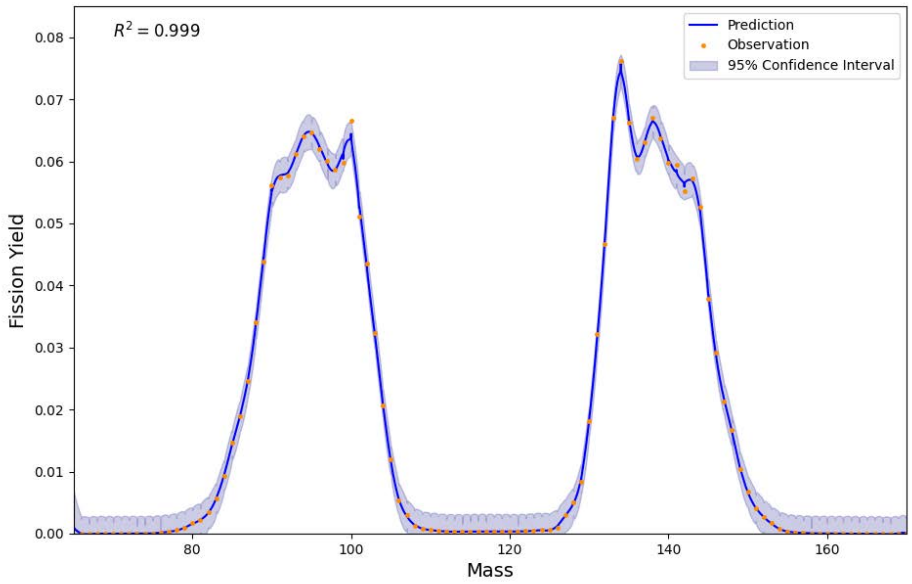

FIGURE 3.5: The mass yield prediction of GPR for Induced fission of ^{235}U

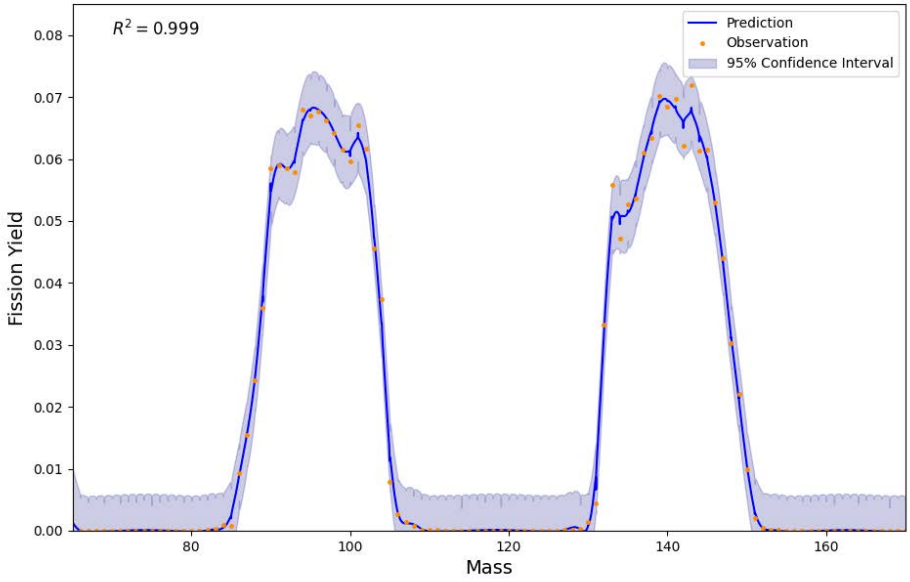

FIGURE 3.6: The mass yield prediction of GPR for Spontaneous fission of ^{238}U

Figs. 3.5, 3.6 show that spontaneous fission exhibits a larger deviation in its function. Although the prediction accuracy was commendable, the confidence interval had to be expanded significantly to accommodate all the data points that were not precisely captured by the prediction. This larger confidence interval indicates a greater uncertainty in the model's predictions for spontaneous fission, reflecting the inherent complexity of the data associated with this type of nuclear reaction.

The inclusion of ^{246}Cm in both its induced and spontaneous fission forms is an important task in order to compare the different fission processes. This particular set holds significant importance in evaluating differences in distribution accuracy and confidence intervals between the two fission types for an isotope sharing the same mass number. Through the analysis of ^{246}Cm under both scenarios, valuable insights are earned into the varying behavior of the same element under distinct fission processes. This comparative assessment is critical in clarifying the correlations of nuclear reactions and can offer crucial insights into the differences that the induced and spontaneous fission has.

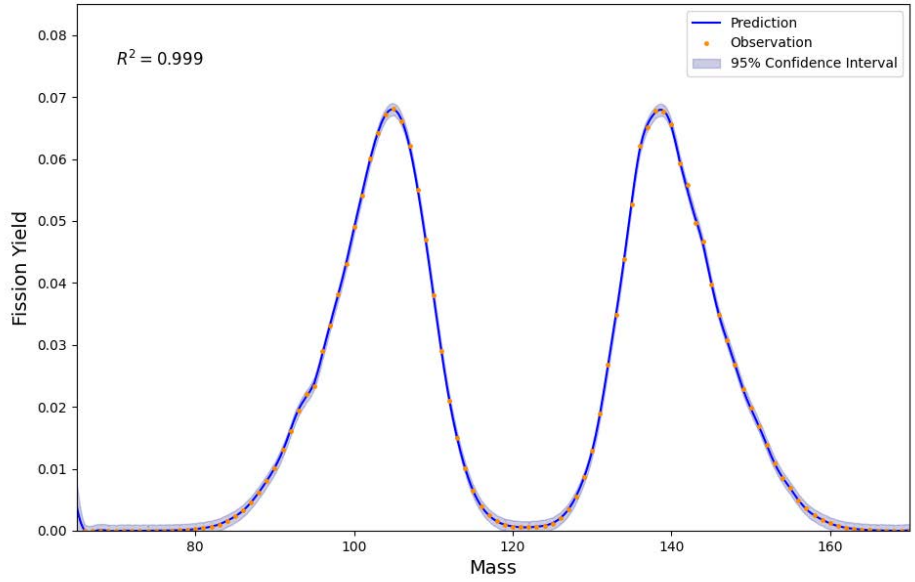

FIGURE 3.7: The mass yield prediction of GPR for Induced fission of ^{246}Cm

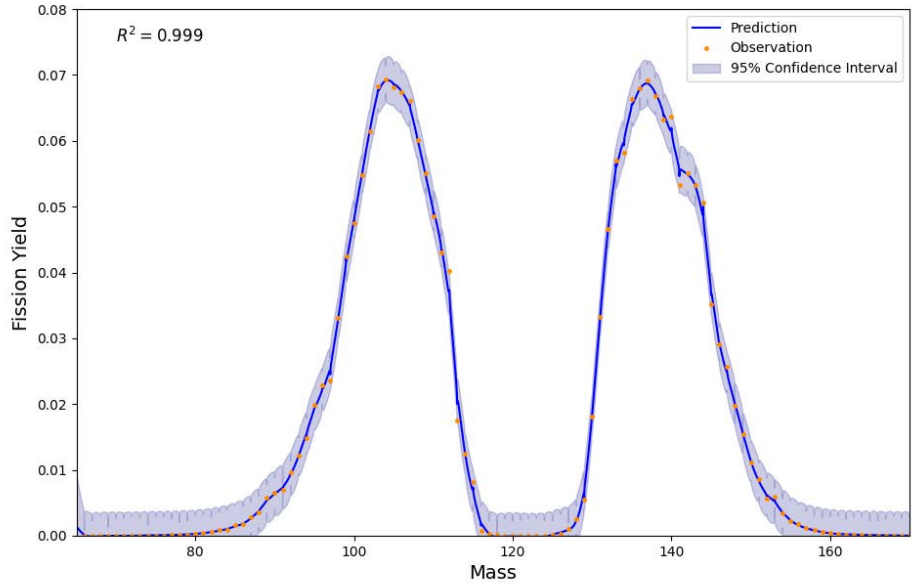

FIGURE 3.8: The mass yield prediction of GPR for Spontaneous fission of ^{246}Cm

The results of ^{246}Cm, under both induced and spontaneous fission conditions, show that the predictions were nearly flawless in both scenarios, yet they differ in terms of uncertainty. In the case of induced fission, the prediction reached an optimal level, characterized by an exceptionally narrow confidence interval. This made it the most accurate prediction of mass yields achieved in this study. Conversely, for

spontaneous fission, while the prediction effectively captured the data distribution with minimal errors, the confidence interval was significantly larger compared to the induced scenario. This indicates a greater level of uncertainty in the predictions for spontaneous fission, despite its overall good performance.

3.2.2 Charge Yields

In addition to the mass yields, the study of charge yield present another main aspect of understanding nuclear fission. Charge yield predictions estimate the distribution of the atomic number of fission fragments resulting from nuclear reactions. This is particularly important in nuclear physics as it provides insights into the charge distribution post-fission. The accuracy of these distributions is essential for various applications, such as the development of nuclear reactors and the management of nuclear waste. By employing advanced predictive models, we can gain a shperical view of the nuclear fission process, including not only the mass but also the charge characteristics of the fission products.

The nuclei that are being used for analyzing the charge yields undergo both spontaneous and induced fission. For induced fission, the cases analyzed are Curium-244 (^{244}Cm) at a neutron energy of 0.5 MeV, Fermium-255 (^{255}Fm) at thermal neutron energy, Uranium-233 (^{233}U) at 14 MeV neutron energy, ^{235}Uat 14 MeV neutron energy, Plutonium-239 (^{239}Pu) also at 14 MeV neutron energy and Fermium-256 (^{256}Fm) for the spontaneous fission.

At the beginning of our analysis, we adapted the GPR algorithm to better align with the predictions of charge yields. The initial fissioning nuclei examined are ^{244}Cm undergoing induced fission at a neutron energy of 0.5 MeV, and ^{239}Pu with neutron energy at 14 MeV. The findings are shown in Figs. 3.9, 3.10.

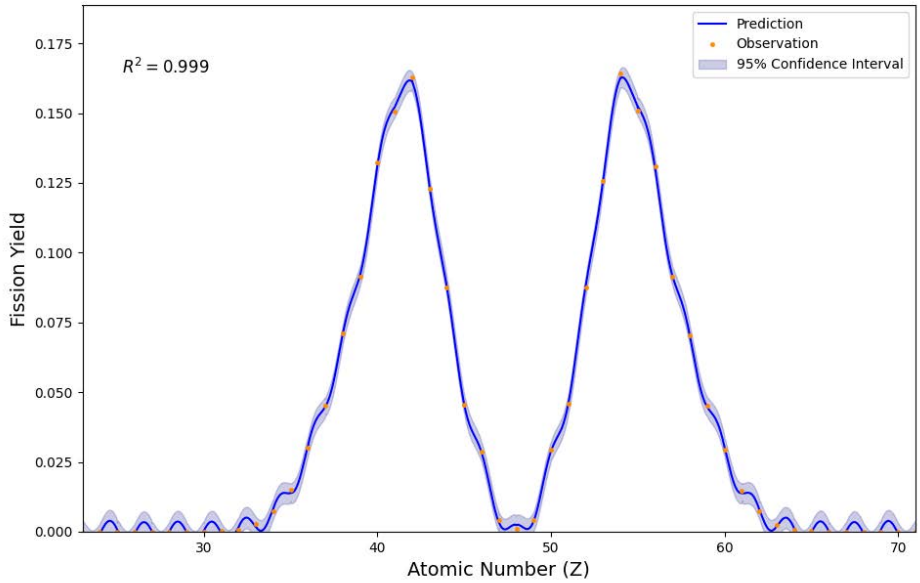

FIGURE 3.9: The charge yield prediction of GPR for Induced fission of ^{244}Cm

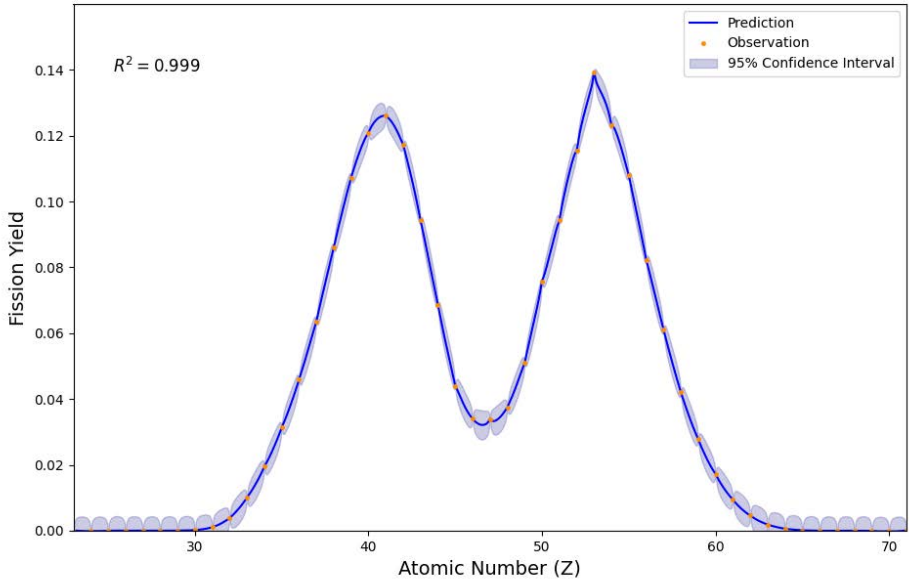

FIGURE 3.10: The charge yield prediction of GPR for Spontaneous fission of ^{239}Pu

The results indicate that we do not obtain the same level of accuracy for charge yields as we did for the mass yields. This discrepancy is primarily attributed to the size of the datasets; the charge yield datasets are approximately half the size of those for mass yields. Even with a method as robust as GPR, accurately predicting charge yields and calculating uncertainties becomes challenging when working with smaller datasets. The limited data size poses significant constraints on the model's ability to learn and make precise predictions, reflected to the relative underperformance in charge yield predictions compared to mass yields. Even if the regression of ^{244}Cm wasn't good enough we can observe the gaussian distributions fitted between the data points, the ^{239}Pu did a better job even though the confidence interval had the same output as in ^{244}Cm.

Figs. 3.11, 3.12 include the induced fission of ^{255}Fm with thermal neutrons, and the spontaneous fission of ^{256}Fm. The analysis compares the fission behavior of Fermium isotopes under different conditions, with one exposed to thermal neutrons for induced fission, and the other undergoing spontaneous fission.

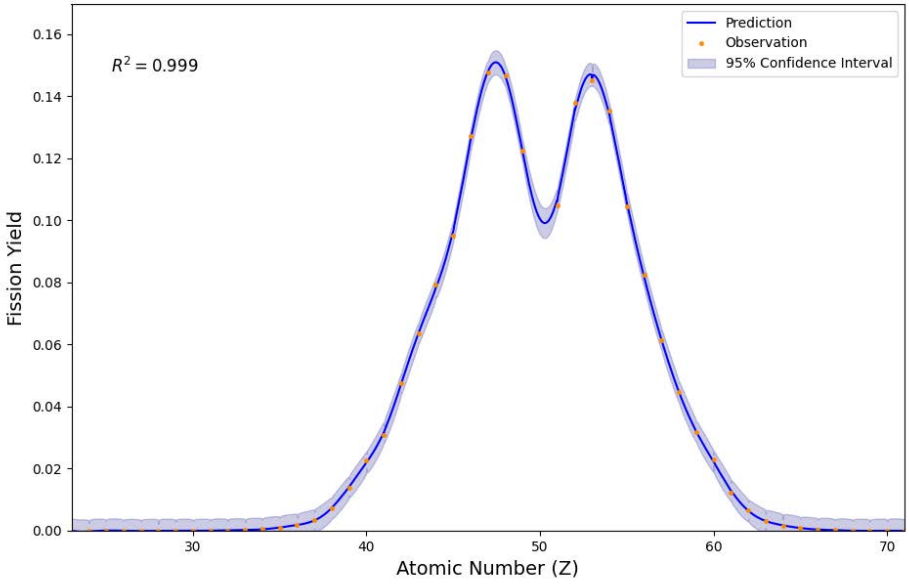

FIGURE 3.11: The charge yield prediction of GPR for Induced fission of ^{255}Fm.

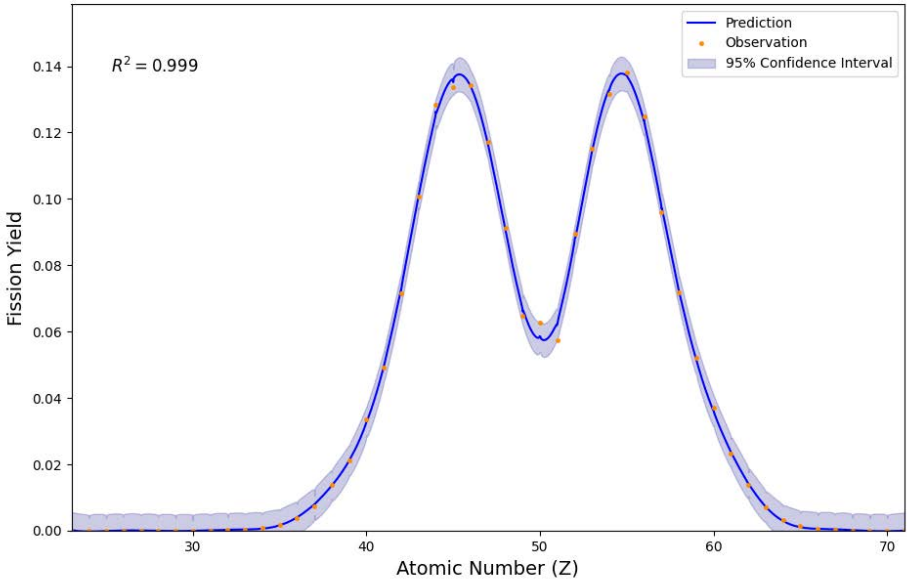

FIGURE 3.12: The charge yield prediction of GPR for Spontaneous fission of ^{256}Fm.

The results show that the different fission types of Fm isotopes in both induced and spontaneous fission scenarios were remarkably similar, showing quite accurate predictions despite the limited size of the dataset for charge yields. The most notable distinction between Figs. 3.11, and 3.12 for these two types of fission lies in the confidence intervals. The confidence interval for the spontaneous fission of Fm was

marginally larger compared to that of the induced fission. However, this difference in the confidence intervals was subtle and barely perceptible. This similarity in the prediction quality, especially under the constraint of smaller datasets, underscores the robustness of the predictive model used for both induced and spontaneous fission scenarios.

The final dataset examined are Uranium isotopes charge yields. Specifically, the induced fission of ^{233}U and ^{235}U, both subjected to neutron bombardment at an energy level of 14 MeV. This focus on Uranium, particularly these isotopes under high-energy neutron conditions, is crucial for understanding the nuances of charge yield distributions in a key element used in nuclear reactions. The analysis of ^{233}U and ^{235}U under these conditions provides valuable insights into the behavior of Uranium in high-energy fission scenarios, which is significant for both theoretical studies and practical applications in nuclear physics.

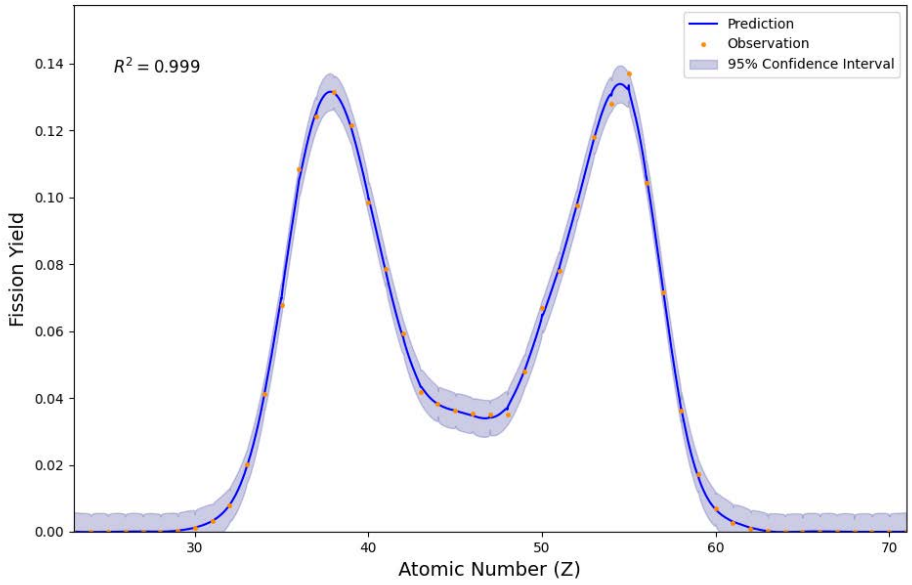

FIGURE 3.13: The charge yield prediction of GPR for Induced fission of ^{233}U

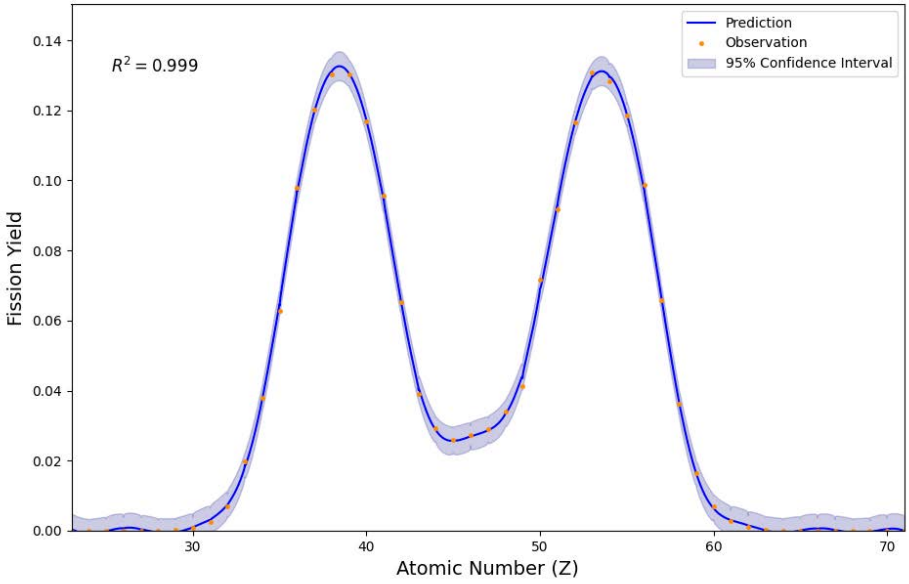

FIGURE 3.14: The charge yield prediction of GPR for Spontaneous fission of ^{235}U

In Figs. 3.13, 3.14, can be distincted that the results for Uranium, specifically for the induced fissions of ^{233}U and ^{235}U at 14 MeV neutron energy, are strikingly similar to those observed for Fermium. The distribution of data points in these cases is sufficiently robust, facilitating accurate predictions of the yields. Equally impressive is the confidence interval, which aligns well with the quality of the outcomes. This consistency in both the yield distribution and the confidence intervals underscores the effectiveness of the predictive model, particularly in handling isotopes like Uranium in high-energy fission scenarios. The reliable data point distribution plays a crucial role in ensuring the precision of these predictions, highlighting the importance of having a well-represented dataset in nuclear fission studies.

Throughout the study of both mass and charge yields, the achieved results were remarkably precise. However, there were a few exceptions where the datasets, such as those for ^{244}Cm and ^{239}Pu in the charge yields, deviated slightly from this trend. This deviation can be attributed to the unusual scattering patterns observed in the data points, coupled with the limited number of observations available for these isotopes. Such factors introduce challenges in achieving high accuracy.

Particularly noteworthy was the performance in the case of ^{238}U. Although the prediction for ^{238}U was close to perfect in terms of the central tendency of the data, there was a significant amount of uncertainty around these data points. This larger uncertainty indicates a higher level of unpredictability or variability in the dataset, which can be a crucial factor for consideration in nuclear physics research. Despite these challenges, the overall high accuracy obtained across most datasets underscores the effectiveness of the methodologies employed in predicting fission yields, both in terms of mass and charge.

The accuracy of the model opens up exciting possibilities for further enhancement. Samples generated by this model's prediction can be utilized as inputs into a larger probabilistic neural network to enhance the fission product yields. While this study does not specifically emphasize the utilization of complex neural networks,

the subsequent section will be dedicated to comparing samples obtained from two distinct methods: the Gaussian Mixture Model and Gaussian Process Regression.

This comparison aims to ascertain which method provides a superior set of samples. By examining the quality and effectiveness of the samples obtained from both GMM and GPR, we will gain valuable insights into the comparative strengths and weaknesses of each method in terms of probabilistic modeling and sample generation. This analysis is vital for informing future research directions and applications, particularly in the context of employing advanced neural network models for predictive accuracy in the field of nuclear physics.

3.3 Kernel Density Estimation

By implementing GPR for prediction, uncertainty estimation, and sample generation, alongside GMM for sample generation through its clustering technique, we have effectively created a substantial pool of samples. These samples are well-suited for training a complex neural network. The accuracy of the samples can be assessed by determining the distribution that best aligns with the experimental data. To evaluate which method is best in capturing the distribution of the data, we conducted a comparative analysis.

The comparison of the sampling datasets was conducted using the Kernel Density Estimation (KDE) method. As a non-parametric approach, KDE is incomparable in statistical analysis for estimating the probability density function of a random variable. Its utility lies in its ability to smooth sample data, offering a clear visualization of the underlying distribution. This is particularly advantageous when the precise form of the distribution is not known or cannot be easily defined. By employing KDE in the comparison process, we can obtain a more insightful understanding of how well the samples from different methods, such as GPR and GMM, represent the true distribution of the data, especially for these kind of datasets that represent multi-modal distributions. This approach ensures a thorough and accurate assessment of the sampling methods' effectiveness in capturing the essential characteristics of the dataset.

This analysis involved plotting the density of the fission yields from the experimental dataset against the densities of the samples generated by both GPR and GMM. By visually comparing these density plots, we aim to identify which method mirrors best the experimental data's distribution. This approach is crucial in determining the effectiveness of each method in representing the true nature of the data, thereby providing insights into their suitability for future applications in predictive modeling.

3.3.1 Mass Yield Density Distribution

We initially focused on the analysis of mass yields of 6 cases of fissioning nuclei, including spontaneous and induced fission at different neutron energies. This abundance of data points is likely to enhance the precision and reliability of the sampling methods, offering a more accurate reflection of the experimental observations.

Starting our analysis, the initial set of samples involves ^{252}Cf and ^{232}Th. The predictions made by GPR are impressively accurate, as evident in figures 3.3 and 3.4. The primary distinction observed is in the size of the confidence interval; the results for ^{232}Th exhibit a larger confidence interval compared to those for ^{252}Cf.

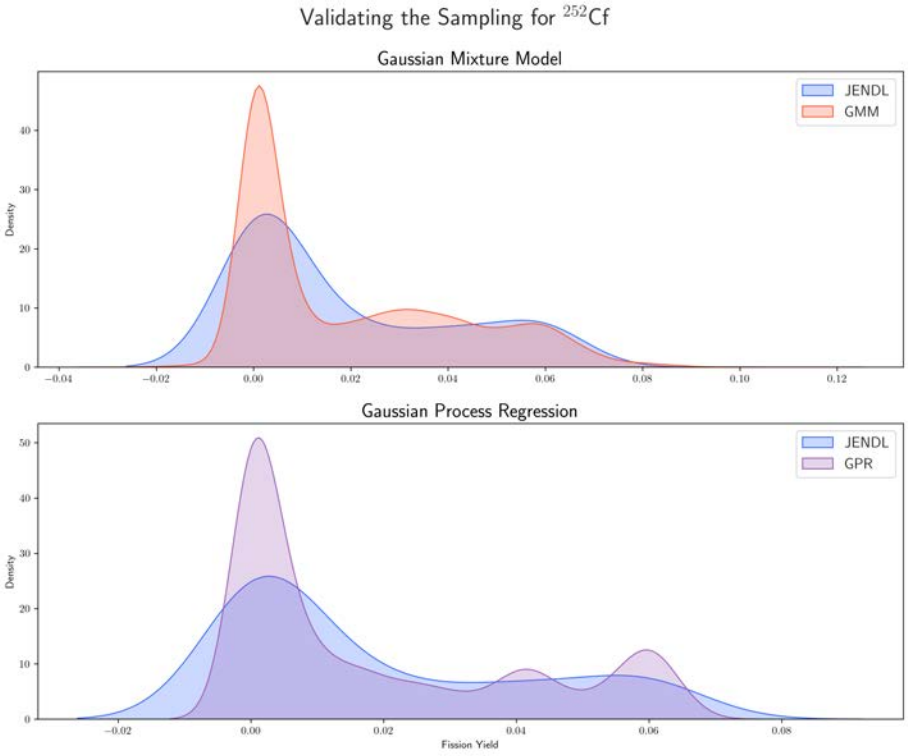

FIGURE 3.15: Evaluation of the mass yield sampling of ^{252}Cf for the methods GMM and GPR

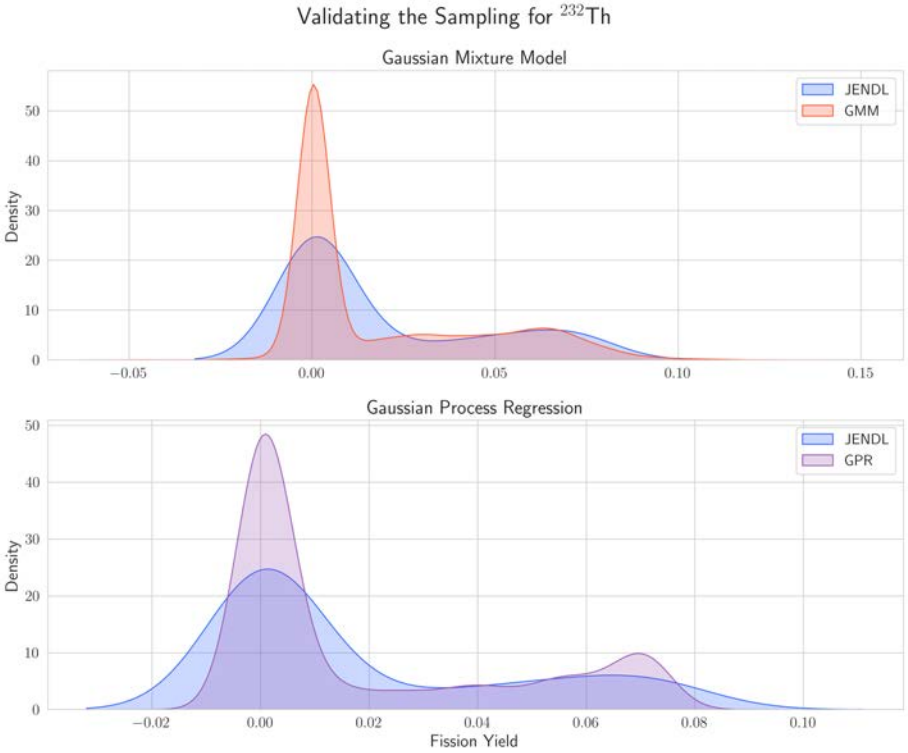

FIGURE 3.16: Evaluation of the mass yield sampling of ^{232}Th for the methods GMM and GPR

Figs. 3.15, 3.16, show the accuracy of the mass yield samples that are extracted is notably higher than that of the charge yields, at least for the first two cases. To discern the difference, a closer look at the center of each figure is informative. Here, we can observe that the density lines for both the experimental data and the sampling data are almost identical. This similarity in density at the core of the figures indicates that the sampling methods employed for these mass yield datasets have been highly effective in capturing the distribution.

For the subsequent set of sampling datasets, we shift our focus to the ^{246}Cm nucleus, comparing induced with spontaneous fission. This comparison offers a unique opportunity to closely examine the accuracy of the GPR sampling, particularly in light of the small confidence interval observed in the induced fission of ^{246}Cm and its highly accurate prediction. The reduced confidence interval in the induced fission case may provide clearer insights into the precision and reliability of the GPR model. This contrast with the spontaneous fission scenario, where the model's performance can be assessed under different conditions, will further our understanding of the GPR's capabilities in capturing the nuances of nuclear fission processes in various settings.

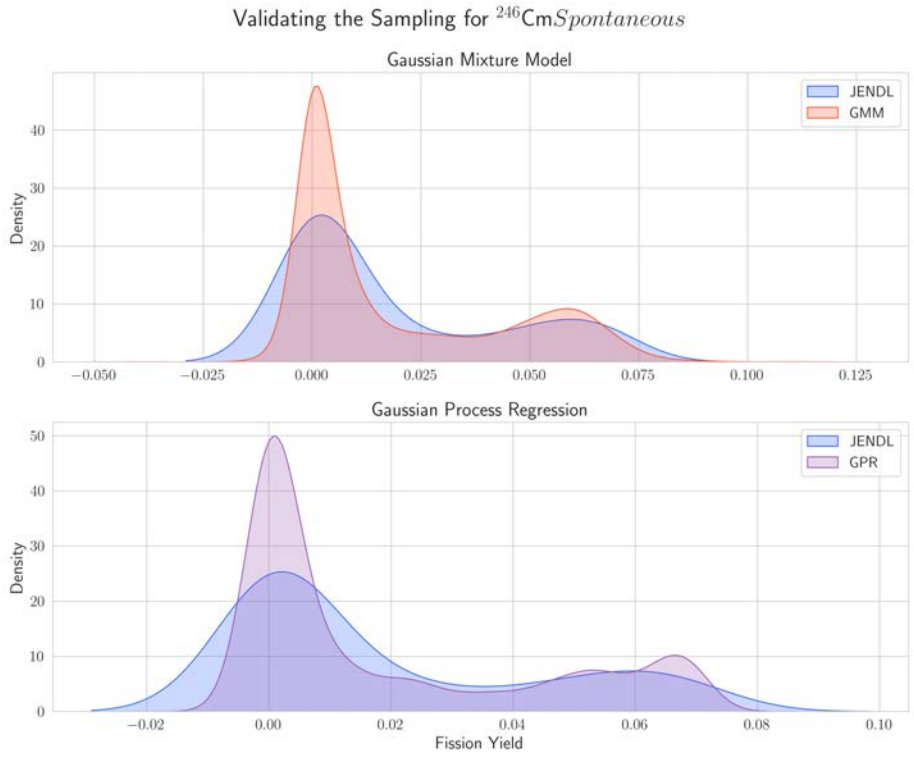

FIGURE 3.17: Evaluation of the mass yield sampling of Spontaneous ^{246}Cm for the methods GMM and GPR

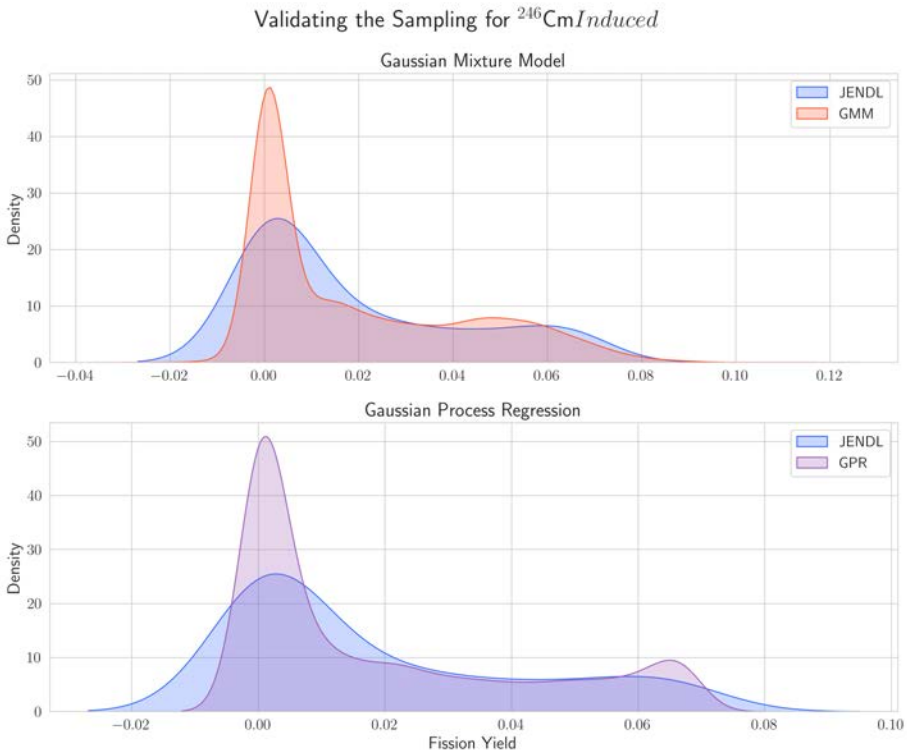

FIGURE 3.18: Evaluation of the mass yield sampling of Induced ^{246}Cm for the methods GMM and GPR

The results clearly demonstrate that the GPR excelled in accurately capturing the distribution of ^{246}Cm, particularly excelling in the induced fission scenario. This high level of accuracy, even in the presence of minor deviations inherent to the methods, suggests that the precision achieved is more than satisfactory. Such performance indicates that we have a robust and reliable sampling dataset at our disposal. The effectiveness of GPR, especially in the context of induced fission for ^{246}Cm, highlights its utility and precision as a tool for nuclear physics research, capable of producing highly competent datasets for advanced analysis and applications.

Finally, we turn our attention to the induced and spontaneous fission yields of Uranium, focusing specifically on ^{235}U and ^{238}U. From our analysis, GPR demonstrated remarkable capability in accurately capturing the mass yield distributions. However, when it came to mass yields, the performance varied. While the predictions for ^{235}U were undeniably accurate, the results for ^{238}U did not reach the same level of precision. This discrepancy indicates that while GPR is highly effective in certain contexts, its performance can vary depending on the specific characteristics and complexities of the dataset, as evidenced by the differing results between ^{235}U and ^{238}U in mass yield outcomes.

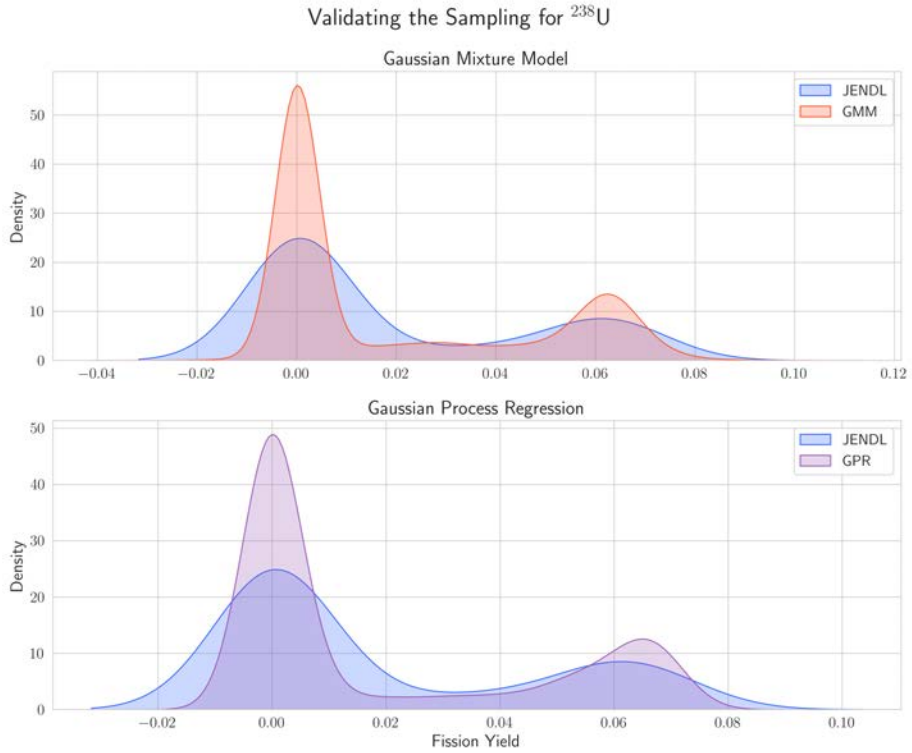

FIGURE 3.19: Evaluation of the mass yield sampling of Spontaneous ^{238}U for the methods GMM and GPR

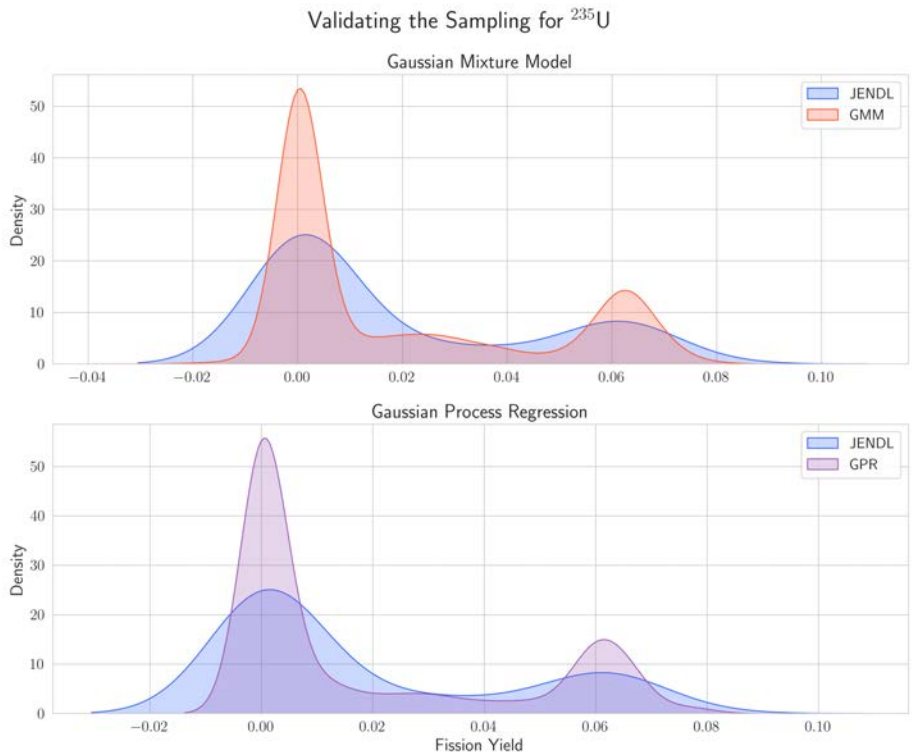

FIGURE 3.20: Evaluation of the mass yield sampling of Induced ^{235}U for the methods GMM and GPR

The analysis reveals that in terms of density of fission yields, the sampling of ^{238}U using GPR yielded better results compared to ^{235}U. Despite the fact that the overall accuracy and confidence interval for Uranium were not as high as those for Curium, GPR still managed to outperform the GMM in the sampling process. This indicates that GPR, while having certain limitations in obtaining good accuracy for Uranium, is particularly better in accurately capturing the density distribution in the fission yield samples.

Summarizing, is evident that GPR has demonstrated a superior capability in capturing the distributions of both mass and charge yields, surpassing the performance of GMM. This distinction in performance was consistently maintained even though the charge yield datasets were limited to half the number of data points compared to the mass yields. Notably, the adequacy of results from the charge yields, despite the reduced data volume, underscores the efficacy of GPR in handling datasets of varying sizes.

A critical advantage of GPR lies in its inherent ability to incorporate the uncertainty present within the dataset into the sampling process. This integration of uncertainty is a potential predictor of even more refined and accurate outcomes in future applications. As such, the GPR sampling methodology stands out as a particularly promising tool in the field of nuclear physics, offering enhanced precision and reliability in predictive modeling. This capability to account for and adapt to the inherent uncertainties in nuclear datasets positions GPR as a highly valuable technique for advancing research and applications in this domain.

3.3.2 Charge Yield Density Distribution

Next, we evaluated the charge yields of 6 fission cases. Given the limited number of data points, this thesis will be particularly insightful. We aim to determine if there are discernible differences in how effectively the sampling methods capture the distribution of the charge yields, compared to the mass yields. This comparison is crucial as it will reveal the impact of dataset size on the ability of methods like GPR and GMM to accurately represent the underlying distribution. By closely analyzing the charge yields, we can gain better understanding of the challenges and limitations faced in situations with sparse data and how these might affect the fidelity of the sampling process.

First, we analyze the charge yields in case of ^{244}Cm and ^{239}Pu. These particular cases are notable as they represent the areas where the GPR model was less accurate. Highlighted in the figures 3.9 and 3.10, these instances are crucial for understanding the model's limitations, especially in complex or challenging datasets. By examining these results, we aim to identify key areas for improvement and gain a deeper understanding of the model's predictive capabilities under various conditions.

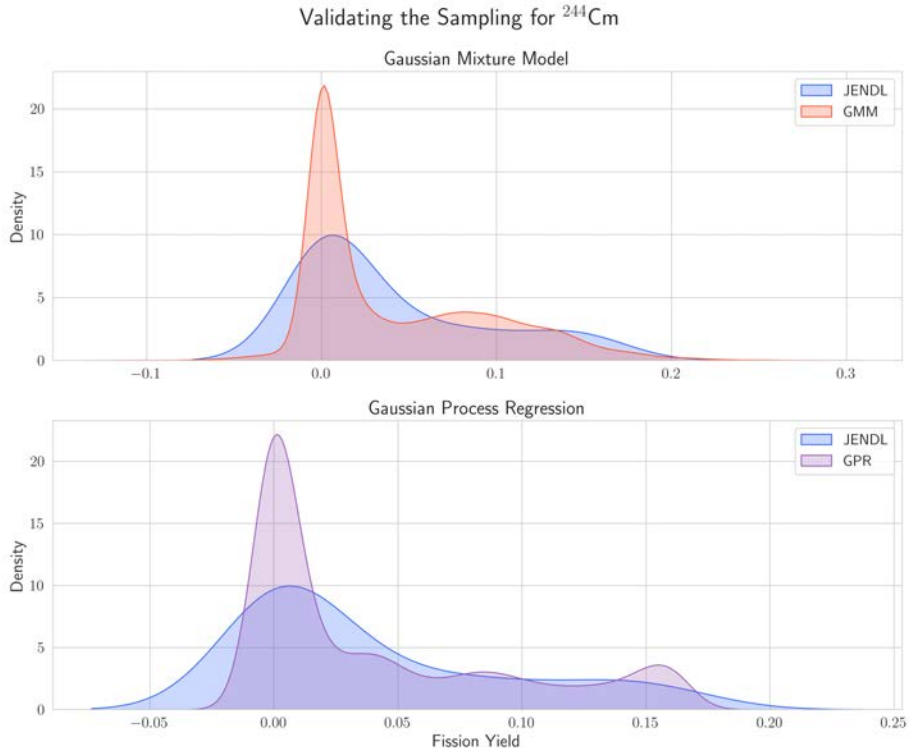

FIGURE 3.21: Evaluation of the charge yield sampling of ^{244}Cm for the methods GMM and GPR

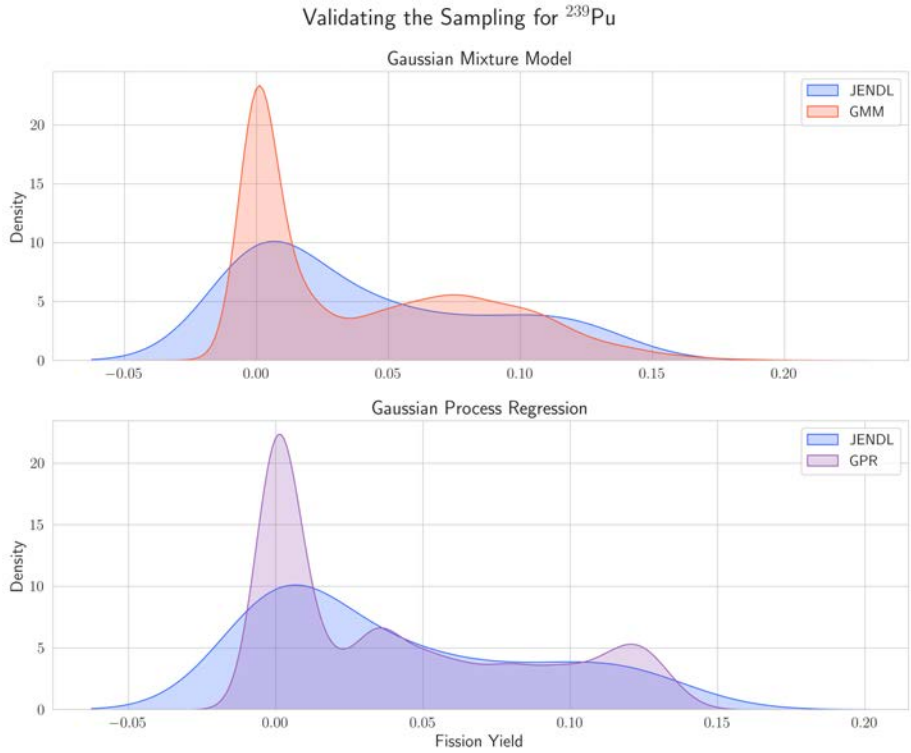

FIGURE 3.22: Evaluation of the charge yield sampling of ^{239}Pu for the methods GMM and GPR

The Figs. 3.21 and 3.22 show that both methods were effective in capturing the distribution of the data. However, the GPR method showed a slight edge in performance. This is noteworthy, especially considering that the overall regression accuracy of GPR wasn't exceptionally high. The ability of GPR to better approximate the distribution, despite its limitations in regression precision, underscores its robustness and potential effectiveness in handling complex data scenarios.

Moving on to the next set of samples, which were among the best in this study, we focus on the results for Fermium, specifically ^{255}Fm and ^{256}Fm. As observed from the figures 3.11 and 3.12, these predictions for Fermium isotopes stood out in terms of their accuracy and precision.

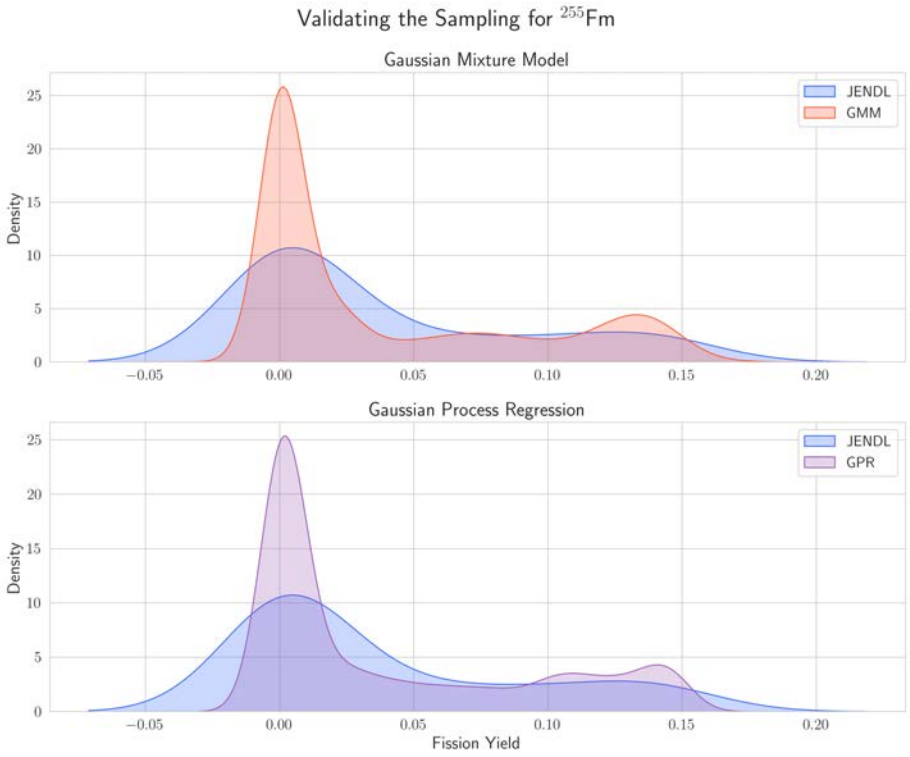

FIGURE 3.23: Evaluation of the charge yield sampling of ^{255}Fm for the methods GMM and GPR

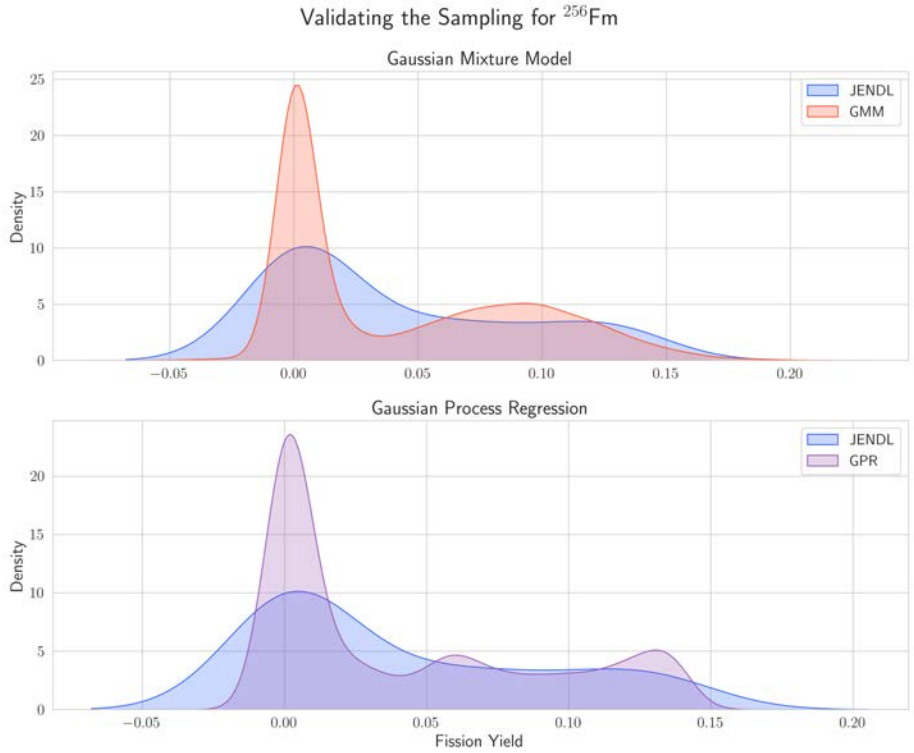

FIGURE 3.24: Evaluation of the charge yield sampling of ^{256}Fm for the methods GMM and GPR

The remarkable accuracy of the GPR predictions for Fermium isotopes theoretically positions it to align closely with the JENDL dataset. Despite the relative simplicity of the GMM, it's noteworthy that it the accuracy of the sampling was close to the GPR, even with the high accuracy it made of the fission yields. This outcome highlights the efficiency and effectiveness of GPR in capturing the nuances of nuclear data.

For the last set of data used for sampling in charge yields we used the Uranium isotopes, ^{233}U and ^{235}U. On the figures 3.13 and 3.14, we saw that the GPR did a slightly worse job at predicting the fission yields than the Fermium isotopes, but only due to the bigger confidence interval that the Uranium had. Hence, we could predict the results of the sampling comparison ourselves:

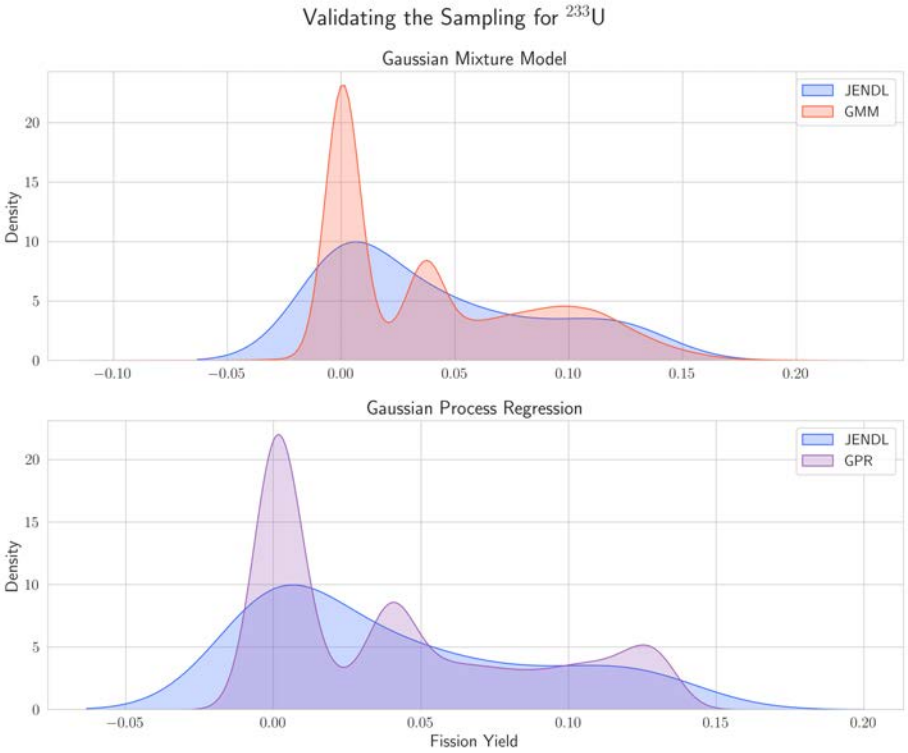

FIGURE 3.25: Evaluation of the charge yield sampling of ^{233}U for the methods GMM and GPR

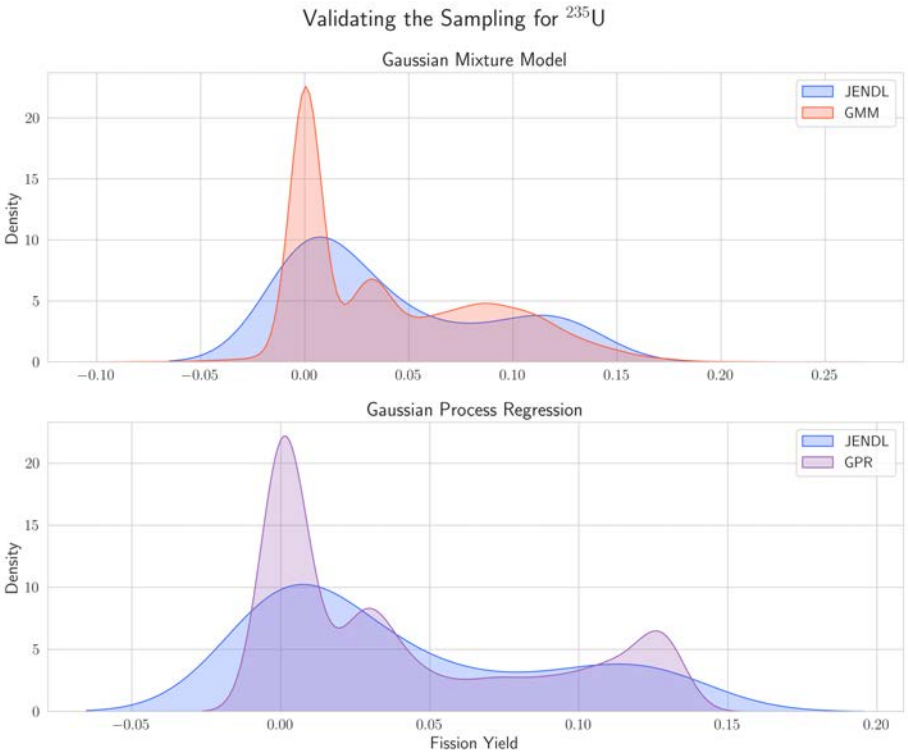

FIGURE 3.26: Evaluation of the charge yield sampling of ^{235}U for the methods GMM and GPR

Analyzing the outcomes of both sampling techniques, it's evident that both are effective in determining fission yields, with GPR demonstrating marginally superior precision. However, GPR's primary limitation is its reduced accuracy at higher fission yield values compared to GMM. This limitation primarily stems from the sampling method employed in the GPR library, which offers the advantage of quantifying the inherent uncertainty in the training data. While this uncertainty may introduce some noise into the dataset, the sophisticated nature of the GPR model allows for enhanced predictive performance when utilizing the GPR-sampled dataset.

3.4 Conclusion

In conclusion, our investigation focused on enhancing the JENDL datasets of mass and charge fission yields using machine learning techniques. We have employed the Gaussian Mixture Model and the Gaussian Process Regression method to extract 10,000 samplings for 12 cases of fissioning nuclei. In the GMM model the only crucial hyperparameter for the model's fitting is the number of gaussians being used for the clustering method. The method itself was succesful and had minimal computational cost, however GMM faced limitations in optimal classification. In order to address this setback, we shifted our focus to GPR, chosen for its prowess in regression tasks and capability to extract uncertainties directly from the dataset. The use of GPR has provided valuable insights into the quality of samples extracted from the dataset. High accuracy and small confidence intervals are indicative of the high quality samples obtained with the GPR compared to those from the GMM. Even in cases where GPR did not capture the data distribution optimally, the option to include confidence intervals in the samples ensured a level of uncertainty estimation. However, it's important to acknowledge the computational challenges associated with GPR, particularly with large datasets, as a kernel method algorithm.

The samplings extracted from both GMM and GPR have been subjected to Kernel Density Estimation to visually assess their ability to capture the distribution of fission yields. The results revealed that GPR consistently produced the highest-quality samples, as evidenced by clearer peaks and denser distributions. This underlines the effectiveness of GPR in enhancing the JENDL datasets and its potential for future applications in nuclear fission research.

This thesis addresses the scarcity of fission yields and aims to identify the most effective method for capturing the distribution of the dataset and extracting high-quality samples. These samples could serve as valuable inputs for more complex probabilistic neural networks like Bayesian Neural Networks and Mixture Density Networks. By incorporating additional parameters such as excitation energy or the charge and mass of the fissioning nucleus, these networks could potentially predict properties of nuclei for which experimental data are lacking, or improve existing theoretical models hindered by computational limitations. The implications of this thesis extend beyond fundamental nuclear research studies, impacting areas such as energy production, and medical technology. Furthermore, it fosters interdisciplinary collaboration, opening pathways to future scientific breakthroughs. This work underscores the transformative potential of machine learning in revolutionizing nuclear fission data analysis, bridging gaps in data scarcity and paving the way for groundbreaking advancements that could reshape nuclear research and its applications in the modern world.

Bibliography

[1] O. Hahn and F. Strassmann. "Über den Nachweis und das Verhalten der bei der Bestrahlung des Urans mittels Neutronen entstehenden Erdalkalimetalle". In: *Naturwissenschaften* 27.1 (1939), p. 11. ISSN: 1432-1904. DOI: 10.1007/BF01488241. URL: https://doi.org/10.1007/BF01488241.

[2] Lise Meitner and O. R. Frisch. "Disintegration of Uranium by Neutrons: a New Type of Nuclear Reaction". In: *Nature* 143.3615 (1939), p. 239. ISSN: 1476-4687. DOI: 10.1038/143239a0. URL: https://doi.org/10.1038/143239a0.

[3] N. Schunck and L. M. Robledo. "Microscopic Theory of Nuclear Fission: A Review". In: *Reports on Progress in Physics* 79 (2016), p. 116301.

[4] Karl-Heinz Schmidt and Beatriz Jurado. "Review on the progress in nuclear fission". In: *Reports on Progress in Physics* 81 (2018), p. 106301.

[5] Michael et al. Bender. "Future of nuclear fission theory". In: *Journal of Physics G: Nuclear and Particle Physics* 47 (2020), p. 113002.

[6] J.H. Hamilton, S. Hofmann, and Y.T. Oganessian. "Search for Superheavy Nuclei". In: *Annual Review of Nuclear and Particle Science* 63.1 (2013), pp. 383–405. ISSN: 0163-8998. DOI: 10.1146/annurev-nucl-102912-144535. URL: https://doi.org/10.1146/annurev-nucl-102912-144535.

[7] J. C. Pei et al. "Fission Barriers of Compound Superheavy Nuclei". In: *Phys. Rev. Lett.* 102 (19 2009), p. 192501. DOI: 10.1103/PhysRevLett.102.192501. URL: https://link.aps.org/doi/10.1103/PhysRevLett.102.192501.

[8] Th. A. Mueller et al. "Improved predictions of reactor antineutrino spectra". In: *Phys. Rev. C* 83 (5 2011), p. 054615. DOI: 10.1103/PhysRevC.83.054615. URL: https://link.aps.org/doi/10.1103/PhysRevC.83.054615.

[9] Joel de Jesús Mendoza-Temis et al. "Nuclear robustness of the *r* process in neutron-star mergers". In: *Phys. Rev. C* 92 (5 2015), p. 055805. DOI: 10.1103/PhysRevC.92.055805. URL: https://link.aps.org/doi/10.1103/PhysRevC.92.055805.

[10] M. et al. Eichler. "The role of fission in neutron star merger and its impact on the r-process peaks". In: *The Astrophysical Journal* 808 (2015), p. 30.

[11] M.B. Chadwick et al. "ENDF/B-VII.1 Nuclear Data for Science and Technology: Cross Sections, Covariances, Fission Product Yields and Decay Data". In: *Nuclear Data Sheets* 112.12 (2011), pp. 2887–2996. ISSN: 0090-3752. DOI: https://doi.org/10.1016/j.nds.2011.11.002. URL: https://www.sciencedirect.com/science/article/pii/S009037521100113X.

[12] Keiichi SHIBATA et al. "JENDL-4.0: A New Library for Nuclear Science and Engineering". In: *Journal of Nuclear Science and Technology* 48.1 (2011), p. 1. ISSN: 0022-3131. DOI: 10.1080/18811248.2011.9711675. URL: https://doi.org/10.1080/18811248.2011.9711675.

[13] Nuclear Energy Agency. *JEFF Nuclear Data Library*. https://www.oecd-nea.org/dbdata/jeff/. n.d.

[14] ZG Ge et al. "The Updated Version of Chinese Evaluated Nuclear Data Library (CENDL-3.1)". In: *Journal of the Korean Physical Society* 59 (2011), pp. 1052–1056. DOI: 10.3938/jkps.59.1052. URL: https://doi.org/10.3938/jkps.59.1052.

[15] C. Simenel and A.S. Umar. "Heavy-ion collisions and fission dynamics with the time-dependent Hartree–Fock theory and its extensions". In: *Progress in Particle and Nuclear Physics* 103 (2018), p. 19. ISSN: 0146-6410. DOI: https://doi.org/10.1016/j.ppnp.2018.07.002. URL: https://www.sciencedirect.com/science/article/pii/S0146641018300693.

[16] Z. X. Ren et al. "Dynamical Synthesis of ^{4}He in the Scission Phase of Nuclear Fission". In: *Phys. Rev. Lett.* 128 (17 2022), p. 172501. DOI: 10.1103/PhysRevLett.128.172501. URL: https://link.aps.org/doi/10.1103/PhysRevLett.128.172501.

[17] Jie Zhao, and Dario Vretenar. "Time-dependent generator coordinate method study of fission: Dissipation effects". In: *Phys. Rev. C* 105 (5 2022), p. 054604. DOI: 10.1103/PhysRevC.105.054604. URL: https://link.aps.org/doi/10.1103/PhysRevC.105.054604.

[18] D. Regnier et al. "Fission fragment charge and mass distributions in ^{239}Pu(n, f) in the adiabatic nuclear energy density functional theory". In: *Phys. Rev. C* 93 (5 2016), p. 054611. DOI: 10.1103/PhysRevC.93.054611. URL: https://link.aps.org/doi/10.1103/PhysRevC.93.054611.

[19] Ulrich Brosa, Siegfried Grossmann, and Andreas Müller. "Nuclear scission". In: *Physics Reports* 197.4 (5 1990), p. 167. ISSN: 0370-1573. DOI: https://doi.org/10.1016/0370-1573(90)90114-H. URL: https://www.sciencedirect.com/science/article/pii/037015739090114H.

[20] K.-H. Schmidt et al. "General Description of Fission Observables: GEF Model Code". In: *Nuclear Data Sheets* 131 (5 2016), p. 107. ISSN: 0090-3752. DOI: https://doi.org/10.1016/j.nds.2015.12.009. URL: https://www.sciencedirect.com/science/article/pii/S0090375215000745.

[21] Aurel Bulgac et al. "Induced Fission of ^{240}Pu within a Real-Time Microscopic Framework". In: *Phys. Rev. Lett.* 116 (12 2016), p. 122504. DOI: 10.1103/PhysRevLett.116.122504. URL: https://link.aps.org/doi/10.1103/PhysRevLett.116.122504.

[22] Stetcu Ionel Bulgac Aurel Jin Shi. "Nuclear Fission Dynamics: Past, Present, Needs, and Future". In: *Frontiers in Physics* 8 (5 2020), p. 054604. ISSN: 2296-424X. DOI: 10.3389/fphy.2020.00063. URL: https://www.frontiersin.org/articles/10.3389/fphy.2020.00063.

[23] A. Boehnlein et al. "Colloquium : Machine learning in nuclear physics". In: *Reviews of Modern Physics* 105 (5 2021), p. 054604. DOI: 10.1103/RevModPhys.94.031003. URL: https://link.aps.org/doi/10.1103/PhysRevC.105.054604.

[24] A. Lovell et al. "Quantified uncertainties in fission yields from machine learning". In: *Phys. Rev. C* 242 (5 2020), p. 05003. DOI: 10.1051/epjconf/202024205003. URL: https://link.aps.org/doi/10.1103/PhysRevC.105.054604.

[25] P. Shanahan, D. Trewartha, and W. Detmold. "Machine learning action parameters in lattice quantum chromodynamics". In: *arXiv: High Energy Physics - Lattice* 105 (5 2018), p. 094506. DOI: 10.1103/PhysRevD.97.094506. URL: https://link.aps.org/doi/10.1103/PhysRevC.105.054604.

[26] Y. Alanazi et al. "A survey of machine learning-based physics event generation". In: *Phys. Rev. C* 105 (5 2021), pp. 4286–4293. DOI: 10.24963/ijcai.2021/588. URL: https://link.aps.org/doi/10.1103/PhysRevC.105.054604.

[27] Zi-Ao Wang et al. "Bayesian Evaluation of Incomplete Fission Yields". In: *Phys. Rev. Lett.* 123 (12 2019), p. 122501. DOI: 10.1103/PhysRevLett.123.122501. URL: https://link.aps.org/doi/10.1103/PhysRevLett.123.122501.

[28] A. Dave et al. "Empirical Models for Multidimensional Regression of Fission Systems". In: *ArXiv* abs/2105.14645 (5 2021), p. 054604. DOI: 10.1103/PhysRevC.105.054604. URL: https://link.aps.org/doi/10.1103/PhysRevC.105.054604.

[29] A. Lovell, A. Mohan, and P. Talou. "Quantifying uncertainties on fission fragment mass yields with mixture density networks". In: *arXiv: Nuclear Theory* 105 (5 2020), p. 054604. DOI: 10.1088/1361-6471/AB9F58. URL: https://link.aps.org/doi/10.1103/PhysRevC.105.054604.

[30] M. Radaideh, D. Price, and T. Kozlowski. "MODELING NUCLEAR DATA UNCERTAINTIES USING DEEP NEURAL NETWORKS". In: *EPJ Web of Conferences* 105 (5 2021), p. 054604. DOI: 10.1051/EPJCONF/202124715016. URL: https://link.aps.org/doi/10.1103/PhysRevC.105.054604.

[31] Oscar Contreras Carrasco. *Gaussian Mixture Models Explained*. https://towardsdatascience.com/gaussian-mixture-models-explained-6986aaf5a95. Towards Data Science. 2022. DOI: 10.1103/PhysRevC.105.054604. URL: https://link.aps.org/doi/10.1103/PhysRevC.105.054604.

[32] Christopher M. Bishop. *Pattern Recognition and Machine Learning*. Vol. 105. Springer, 2006, p. 054604. DOI: 10.1103/PhysRevC.105.054604. URL: http://users.isr.ist.utl.pt/~wurmd/Livros/school/Bishop-PatternRecognitionAndMachineLearning-Springer2006.pdf.

[33] Kevin P. Murphy. *Machine Learning: A Probabilistic Perspective*. Vol. 105. Cambridge, Mass: MIT Press, 2012, p. 054604. DOI: 10.1103/PhysRevC.105.054604. URL: https://link.aps.org/doi/10.1103/PhysRevC.105.054604.

[34] Cory Maklin. *Gaussian Mixture Models*. https://towardsdatascience.com/gaussian-mixture-models-d13a5e915c8e. Towards Data Science. 2022. DOI: 10.1103/PhysRevC.105.054604. URL: https://link.aps.org/doi/10.1103/PhysRevC.105.054604.

[35] Ding Wei-cheng. "An application of GMM model in nuclear spectrum smoothing filtering". In: *Nuclear Techniques* 105 (5 2010), p. 054604. DOI: 10.1103/PhysRevC.105.054604. URL: https://link.aps.org/doi/10.1103/PhysRevC.105.054604.

[36] A. Lovell et al. "Nuclear masses learned from a probabilistic neural network". In: *Physical Review C* 105 (5 2022), p. 054604. DOI: 10.1103/PhysRevC.106.014305. URL: https://link.aps.org/doi/10.1103/PhysRevC.105.054604.

[37] C. E. Rasmussen and C. K. I. Williams. *Gaussian Processes for Machine Learning*. Vol. 105. The MIT Press, 2016, p. 054604. DOI: 10.1103/PhysRevC.105.054604. URL: https://link.aps.org/doi/10.1103/PhysRevC.105.054604.

[38] Hilarie Sit. *Quick Start to Gaussian Process Regression*. https://towardsdatascience.com/quick-start-to-gaussian-process-regression-36d838810319. Towards Data Science. 2022. DOI: 10.1103/PhysRevC.105.054604. URL: https://link.aps.org/doi/10.1103/PhysRevC.105.054604.

[39] F. Pedregosa et al. “Scikit-learn: Machine Learning in Python”. In: *Journal of Machine Learning Research* 12 (5 2011), pp. 2825–2830. DOI: 10.1103/PhysRevC.105.054604. URL: https://link.aps.org/doi/10.1103/PhysRevC.105.054604.